

In the format provided by the authors and unedited.

Earth's topographic relief potentially limited by an upper bound on channel steepness

George E. Hilley ^{1*}, Stephen Porder², Felipe Aron ³, Curtis W. Baden¹, Samuel A. Johnstone ^{1,4}, Frances Liu¹, Robert Sare ¹, Aaron Steelquist¹ and Holly H. Young¹

¹Department of Geological Sciences, Stanford University, Stanford, CA, USA. ²Department of Ecology and Evolutionary Biology, Brown University, Providence, RI, USA. ³National Research Center for Integrated Disaster Risk Management (CIGIDEN) & Departamento de Ingeniería Estructural y Geotécnica, Pontificia Universidad Católica de Chile, Santiago, Chile. ⁴Present address: United States Geological Survey, Lakewood, CO, USA. *e-mail: hilley@stanford.edu

Expanded Methods

Erosion rates were measured from cosmogenic ^{10}Be concentrations in 14 samples collected across an erosion rate gradient, while approximately controlling for rock type and climate. The 250-500 and 500- 710 μm size fractions were extracted from bulk river sand samples, and ~ 100 g of quartz was isolated using magnetic separation followed by progressive HF/HNO₃ leaches. Next, the quartz was digested with ~ 300 μg of Be carrier, and Be was extracted and oxidized to produce BeO₃. $^{10}\text{Be}/^9\text{Be}$ ratios were measured at Lawrence Livermore National Laboratory's Center for Accelerator Mass Spectrometry and Purdue's PRIME Lab using the calibration in Nishiizumi et al. Background $^{10}\text{Be}/^9\text{Be}$ ratios were measured and applied as follows: Venezuela and Costa Rica samples: $6.26 \pm 0.16 \times 10^{-15}$; Brazil samples: $5.71 \pm 0.58 \times 10^{-15}$; Taiwan and Guatemala samples: $5.69 \pm 7.25 \times 10^{-15}$. Be concentrations were converted to basin-wide averaged denudation rates using the mean catchment elevation and time-dependent corrections of Lal and Stone implemented in version 2.1 of the CRONUS-Earth ^{10}Be - ^{26}Al age calculator (Information used for denudation calculation is presented in Supplementary Table S1). Since the CRONUS-Earth calculator does not account for the spatial variability of production rates that result from both latitudinal changes in basin locations as well as changing elevations throughout the basin, we calculated basin-averaged scaling factors of production rates considering the non-linearity of topography and shielding of cosmic radiation by topography and snow cover. We calculated three pixelwise scaling factors using 100-m-resolution Digital Elevation Model (DEM) based according to scaling scheme of Lal and Stone. First, we considered the scaling factor for the nonlinearity of production rate with elevations, which is calculated from the ratio between production rate based on mean elevation and production rate based on real topography. Second, since some of the studied basins have significant relief and high altitude, we took into account the shielding from topographic obstacles. Topographic shielding was calculated for each pixel as (Dunne, Elmore, and Muzikar 1999) :

$$S_{topo} = 1 - \frac{1}{n} \sum_{i=1}^n \Delta\phi_i \sin^{m+1} \theta_i \quad (\text{S2})$$

where S_{topo} is the shielding factor for topography, n is numbers of segments with an azimuthal angle of the incoming radiation $\Delta\phi_i$ and with an inclination angle from the horizontal θ_i , and an experimental constant $m \sim 2.3$. The 360° shielding factor was calculated for each DEM pixel with 10° steps for the azimuth angle.

Samples were collected from unglaciated catchments to preclude the effects of any large change in erosion rates resulting from the glacial - interglacial transition (Moon et al. 2011). We acknowledge that tropical, nonglaciated catchments are not the only geomorphic environment that may be suitable for this type of analysis. In fact, the requisite condition for performing this type of analysis would be to ensure the erosion had been steady over the integration time of the ^{10}Be dosage, which can range from 100s to 100000s of years, depending on the erosion rate. Our selection of sites within tropical granitic landscapes, by definition, avoids the possibility that these landscapes have undergone a profound, climate-related deglaciation. Given that this

transition can be responsible for substantial changes in erosion rates through time, our site selection seeks to avoid areas that could plausibly have experienced a recent, large-magnitude change in erosion rates. Additionally, 12 / 14 basins selected show $R-2 > 0.7$ values, suggesting that in most cases, a case cannot be made for large transient knickpoints moving through the basins, which would bring into question the assumption of uniformity of incision rates across these basins.

An additional assumption of our analysis is that erosion rates across an entire catchment are uniform and quantitatively match channel incision rates. This assumption is implicitly embedded in all detrital cosmogenic erosion-rate studies that link landscape form with erosion rate. This supposition may be somewhat problematic in slowly eroding catchments where diffusive processes dominate hillslope mass transport, because the response time of hillslopes to changes in base-level lowering rate at the channels may take hundreds of thousands of years to equilibrate across the hillslopes (Fernandes and Dietrich 1997). But, most catchments display slopes that are sufficient to trigger non-linear hillslope transport processes, which dramatically reduces the response time of hillslopes to changes in base-level lowering rate (Roering, Kirchner, and Dietrich 1999). Finally, because the lowest-erosion-rate sites have the longest hillslope response times, we would expect the Venezuelan and Brazilian sites to be most susceptible to hillslopes that are in a disequilibrium with respect to channels. Yet, these sites have been tectonically quiescent for tens-of-millions of years (Larson and Ladd, 1973; de Oliveira Carmo and Vasconcelos, 2006), and so there are few tectonic mechanisms for recently changing rock uplift rates.

The samples we measured in Taiwan are noteworthy from both a measurement and lithologic perspective. First, while we did our best to find rapidly eroding granitic catchments hosted in the appropriate climatic range, we found our best option (in terms of accessibility and appropriateness of high erosion rates) to be the eastern side of the Central Range of Taiwan. However, it is important to acknowledge that the rocks hosted in this environment are not granitoids, but rather metasedimentary rocks. While high-grade variants likely have K values similar to those of granitic rocks (Stock and Montgomery 1999), we cannot rule out the possibility that weaker variants exposed within the sampled catchments may be characterized by values that are lower. Nonetheless, the extrapolation of low-erosion-rate sites to these high erosion rates produces an approximately two-order-of-magnitude discrepancy between k_s values expected for granitic catchments subjected to these high erosion rates and those observed for $n=1$. This would require a two-order-of-magnitude decrease in the value of K in the Taiwanese catchments relative to all other catchments sampled, which is unlikely. This assertion is supported by our global topographic analysis, which finds virtually no points on the planet steeper than $k_s = 200 \text{ m}^{0.8}$, $n=1$. Should we wish to explain the change in steepness as a variation in K value, the implication would be that no catchments underlain by granitic (or comparably low detachability) lithologies have yet been sampled in high erosion-rate environments, nor would these lithologies be present in steep landscapes anywhere on the planet. Thus, when viewed in the context of previous erosion-rate measurements and global

topography, it is unlikely that the low k_s values observed in Taiwan can plausibly be explained by the erodibility of rocks hosted in these landscapes.

The other aspect of the Taiwan erosion rate sites that is worthy of discussion is the fact that analytical uncertainties on the erosion rates are high. This results from the fact that the sampled sands were quartz poor, and the catchments are located at low-latitude, low-elevation sites. The former of these factors required us to process many kilograms of sample to obtain the 150-400 grams of clean quartz used in the digestion. Despite these extreme sample processing steps, the low-production rate, high erosion-rate environment creates fundamental challenges to measuring these ratios with accuracy. Nonetheless, despite the (sometimes) large analytical uncertainties, our erosion-rate estimates are in line with samples collected and published from some overlapping and adjacent basins from the Central Range (Derrieux et al. 2014). Interestingly, within the catchments sampled on Taiwan, short-term erosion rates are similar in magnitude to long-term exhumation of rock inferred using Zircon Fission Track (ZFT) thermochronology (Fellin et al., 2017). This suggests that this portion, and indeed much of the landscape in Taiwan, may be in steady-state (Fellin et al., 2017).

Finally, there is a question as to whether the extremely variable climate in Taiwan, the short time-scales of cosmogenic exposure, and the stochasticity of erosion may cause a systematic mis-estimation of denudation rate and channel steepness in the high-erosion-rate catchments. In particular, it might be argued that the short dosage times, coupled with highly variable erosion rate may bias the rates we obtain from cosmogenic radionuclide analyses. Unfortunately, if correct, this is an intrinsic limitation of the detrital cosmogenic method, and one cannot make a compelling argument around this effect for individual samples. However, if this is the case, it is not uniquely a property of our samples, as there is order-of-magnitude consistency between our Taiwanese sites, and the magnitude of denudation is on par with previously studied samples (discussed above). If these catchments were instead poorly fit by the profile geometry expected from a power-law-type incision rule, we would expect anomalously low $R-2$ values for the morphologic fits of the high-erosion-rate basins, which is not what is observed. Nonetheless, for the case of the high-erosion-rate sites, there is some question as to whether there are systematic biases in our measurement methodologies at these sites that produce the break in scaling.

It is for these reasons that we sought to test this scaling break with global datasets. The fact that the maximum k_s value that we observe in our dataset is the same that is observed in the global dataset provides some independent support for the idea that such a threshold k_s -value may exist. Finally, the fact that exceedingly few points on the surface of our planet have k_s values greater than the maximum value observed in any compilation further bolsters our claim that k_s indeed reaches a maximum value beyond which further increases in denudation rate do not affect relief. Thus, while one might assert that the break in scaling we observed at our sites is the result of systematic biases in the way the topography of the sites are measured, the fact that there is broad consistency of these results with global compilations and the overall topographic structure of our planet makes this explanation unlikely.

Historic precipitation records

To examine the impacts of regional climate on our erosion rate dataset, we compiled historic precipitation records for seven weather stations located near the river-sand sample sites from a variety of data sources (Figure S6). The five stations chosen for the Central and South American sites are part of the Global Historical Climatology Network (GHCN) and record daily precipitation and other meteorological observations (Lawrimore et al. 2011). Data from the two stations nearest the Taiwan sites are derived from six-hourly precipitation measurements reported in the Global Summary of the Day (GSOD) data product. Daily precipitation totals were estimated by summing the six-hourly measurements (PCP06) available for a given day. Both datasets were accessed through the National Centers for Environmental Information of the National Oceanic and Atmospheric Administration (<https://gis.ncdc.noaa.gov/maps/ncei>).

While other data sources exist, the GCHN/GSOD records appear to be the longest records of daily to sub-daily precipitation that are publically available near all of the sample sites. For example, in Taiwan, several stations in the Central Mountain Range record 60 years of precipitation measurements, but these data are not openly accessible (Chu et al. 2014).

Station locations and precipitation records are shown in Supplementary Figures S6 and S7. Stations were selected based on proximity to each sample site and position with respect to major topographic barriers in each region. An attempt was made to select an upland station for each sample site, but no upland stations with accessible data were available for the Taiwan sites. All available data was used, except for the station in Costa Rica, where the initial record from 1977 to 1985 was removed due to anomalous data recording unrealistically high and persistent rainfall for the entire 8-year period. Both data sources contain missing data with various frequencies, including large data gaps over one year long (Figure S7c, d, and e).

While several stations lie in or near the catchment area of each sample site or similar catchments nearby (Figure S6c and d), others are far from the respective sample sites (Figure S6a and b). In these cases, station selection was limited by data availability within the area of interest. For the Guatemala sample site (Figure S6a), the nearest GHCN station in the country is in Guatemala City, and lies at an elevation of 1496 m in a subtropical highland climate zone. A nearby station in Catacamas, Honduras was selected for this site as it occupies a similar elevation to the sample site in a tropical savanna climate zone. For the sample sites in Costa Rica (Figure S6b), two stations are available: a station in Puerto Cortes, near the country's western coast, and an airport weather station in San Jose. This station was selected as the more representative site owing to its position to the east of Costa Rica's continental divide and inland location.

The simple daily intensity index (SDII) was calculated for each record to compare the average precipitation intensities of each site. The SDII is defined as

$$SDII = \frac{\sum_{p \in W} p}{|W|} \text{ where } W = \{ p_i : p_i \geq 1 \text{ mm} \}, \quad (S3)$$

which is the average precipitation on days with at least 1 mm of observed precipitation, referred to as “wet” days (Karl et al. 1999). To summarize the overall climate and magnitude of heavy and extreme events, the mean annual precipitation and the 90th and 99th percentiles of precipitation on wet days for each dataset are given in Table S6. The magnitude of heavy rainfall events (at least 90th percentile) and average daily rainfall were compared by computing the ratio of each peak event’s precipitation to the mean daily precipitation for that year. The time series of peak-to-mean precipitation ratios for each station are shown in Figure S8.

The study sites differ in the magnitude and number of heavy precipitation events and average annual and daily rainfall intensities. Coastal stations in Brazil and Taiwan recorded the highest mean annual precipitations, over 1.5 m in both cases, and the southernmost station in Venezuela recorded the lowest mean annual precipitation (Table S6). The records from Brazil, Costa Rica, and Taiwan yielded the highest SDII values (12.5-14 mm day⁻¹).

Notably, the stations in Taiwan recorded the largest rainfall extremes, with a 99th percentile of 133-137.9 mm compared to a range of 45.0-95.8 for the Central and South American stations. This is also reflected in the maximum peak-to-mean ratios for the Taiwan stations, which are greater than 10 on average (Table S6 and Figure S8g and h). The 90th percentile precipitation ranges from 28.9-39.1 mm in the records from Brazil and Taiwan, whereas it is below 23 mm for all other stations.

Past work describes regional precipitation trends and extremes for some of the study areas. Recent analysis of 60-year precipitation records from Taiwan indicate that Central Weather Bureau stations near the study sites experience mean SDII of 31.6-26.9 mm day⁻¹ during the typhoon season with an average of 7.5 days of rainfall above 50 mm (stations 708, 753, and 755 of Chu et al. 2014). No such studies are available for individual stations during wet seasons in the Central or South American study areas. However, regional studies of precipitation on the southeast coast of Brazil over the past 70 years report a value of SDII (9.7 mm day⁻¹) slightly lower than to those calculated here (Zilli et al. 2017). The same study calculates the 95th percentile daily precipitation intensity and frequency to be 29.1 mm day⁻¹ and 7.1 events year⁻¹, respectively (Zilli et al. 2017). Low values for all indices may be due to averages including inland stations which show a lower frequency and intensity of extreme precipitation events relative to the coastal catchments where sampling occurred (Zilli et al. 2017). Similarly, regional studies of storm events in Costa Rica report an SDII of ~9.6 mm day⁻¹ in the proximity of sample sites, lower than our calculated value of 14 mm day⁻¹ (Rapp et al. 2014).

Effect of precipitation intensity variations on channel steepness

Our study attempted to target sample sites with mean annual precipitation (MAP) values between 1000-1500 mm/yr. We were largely successful in reaching this objective, although the nearest precipitation station to one of the Venezuela sites recorded only ~425 mm/yr of MAP. The site receiving the greatest MAP was Brazil, with ~1880 mm/yr. In each case, sites experiencing high MAP do not show systematically lower channel steepness values, which would be expected based on the increased overall discharge at these sites (Table S6).

MAP is an imperfect measure of climate's impact on channel erosion. In cases where the peak, rather than the mean discharge limits the erosion of channels, environments in which a few, large storms deliver the majority of the mean annual precipitation may be more erosive than environments in which steady, lower-precipitation intensities dominate. The fact that Taiwan's MAP tends to be delivered in only a few, high-intensity events might help to explain the lower channel steepness values observed at that site. In our analysis, the ratio of the maximum precipitation intensity relative to the mean is around 7:1 for the Venezuela, Costa Rica, and Guatemala sites, is around 9:1 for the Brazil site, and is up to 12:1 for Taiwan. Thus, if precipitation intensity is a proxy for relative variations in peak-to-mean discharge ratios, we might expect Taiwan to be about 170% more erosive than the Costa Rica, Guatemala, and Venezuela sites. Brazil would then be about 130% more erosive relative to these reference sites. Our steepness estimates assume uniform precipitation across all sites, allowing watershed area to be used as a proxy for discharge. Steepness, in turn, varies with the watershed area raised to the concavity. If we account for the difference between the maximum and mean annual discharge by scaling watershed area according to the ratio of maximum to mean annual precipitation, channel steepness in Taiwan that would be expected if rainfall occurred during comparable conditions as the reference sites would be 125% of their observed value, for a concavity of 0.4. This 5/4 adjustment in steepness is insufficient to account for the ~2 orders-of-magnitude discrepancy in channel steepness between theory and observations. Finally, the other two sites at which we observed similar steepness to Taiwan (Costa Rica and Guatemala) do not show the same concentration of precipitation in focussed, high-intensity events. Furthermore, the site most similar to Taiwan (in terms of the distribution of precipitation) is Brazil, which does not show the threshold behavior we observe. Thus, while we acknowledge that climate, especially as measured by MAP, is likely an important control on channel steepness, our climate analyses suggest that this factor, by itself, can only explain a small fraction of the discrepancy between erosion rate-steepness values that we measure and those predicted by simple theory.

Fraction of Basins Occupied by Channel Slopes > 0.2

We calculated the fraction of channel slopes within a sampled basin whose along-channel slopes were > 0.2. Channel slope calculations are sensitive to local digital elevation model noise, and so we used an algorithm that calculates channel slopes based on equal vertical elevation intervals. To do this, we extract the channel network from the digital elevation model in a way described in the Methods, using pit-filling and the D8 steepest descent flow path. We then isolated channel links with identical order within the network, and sampled elevations along

each link at an equal elevation interval (in this case, 40 meters was used as the vertical interval to sample beyond the typical vertical elevation noise we observed in the SRTM-90 elevation models. Channel slopes were calculated between points, those greater than 0.2 were identified, and the fraction of these points (relative to the total number of channel points identified by this methodology) was computed for each basin. The results of this analysis are shown in Figure S1.

We observed that the fraction of channel networks dominated by channel slopes > 0.2 , increased with erosion rate, and reached a maximum value of 0.8-1 in the steepest basins. Because portions of the channel network whose channel slopes are > 0.2 are commonly associated with a process transition to debris-flow incision, this observation is not inconsistent with the idea that the initiation of debris flow incision could be responsible for the observed threshold. However, these observations are also consistent with the idea that the fraction of the channel network hosting debris flows is limited by the maximum value of k_s , which may be produced by an entirely different set of processes. Thus, while there is some relationship between this fraction and k_s , it is unclear whether this correlation implies any causality that would allow us to ascribe the limiting value of k_s to the initiation of debris flows in steep landscapes.

Effect of Concavity on Results

We show the effect of concavity on the relationships between erosion rate and steepness for our measured samples in Figures S2 ($\theta=0.5, 0.6$). The magnitude of averaged k_s values increases with concavity, as is required by the change in the dimensions of k_s with concavity. Regardless of the concavity used, we observe that steepness increases with erosion rate until high steepness values have been achieved (the exact value of this limiting steepness value varies with concavity). Fields in Figure S2 equivalent to K-values deduced by Stock and Montgomery (1999) are not shown for $m/n=\theta=0.5$ or $\theta=0.6$ due to the fact that these values were calibrated for $\theta=0.4$ in the previous study and will vary with the value of m and n . Additionally, Stock and Montgomery (1999) found covariance between fitted values of K , m , and n in their calibration study. Thus, one would necessarily have to use their original data to recalibrate values for K , m , and n given $\theta=0.5$ and $\theta=0.6$ to construct fields representing expected erosion rate - steepness relationships for different rock types. Given that the raw data that would be required to recompute these conditional calibrated values were not reported in Stock and Montgomery (1999), we limit the presentation of the lithologic fields in these (and related) plots to the calibrated case of $\theta = 0.4, n = 1$.

We also recomputed erosion rate - steepness relationships for $\theta=0.5, 0.6$ for the global dataset presented by Portenga and Bierman (2011). As with our own systematic sampling, we observed a similar limiting value of averaged k_s in this dataset, regardless of concavity (Figure S3). Thus, our conclusions about a steepness and relief limit appear robust to the range of concavities explored (0.4-0.6), which spans the typically observed range on the planet. In both

datasets, there is no evidence to support the view that the limiting steepness / relief value that we detect is an artifact of the values of concavity that we have used in our analysis.

Finally, we explored the effect of varying concavity on the distribution of steepness that we measured across our planet using the HydroSheds 500-m-resolution dataset (Figure S4, S5). As with our previous analyses, the dimensional nature of k_s requires larger values to produce identical relief as concavity increases. Nonetheless, we observe a global steepness / relief limit that corresponds to the upper limits of averaged k_s observed in both our own systematic sampling, as well as those data presented by Portenga and Bierman (2011). Thus, while concavity necessarily changes the magnitude of k_s , the observation that the upper end of the range of k_s values observed in our systematic sampling also bounds global erosion rate - steepness compilations and the observed values of averaged k_s values on our planet appears robust, despite the value of concavity chosen.

References:

- Chu, Pao-Shin, Den-Jing Chen and Pay-Liam Lin, 2014. "Trends in precipitation extremes during the typhoon season in Taiwan over the last 60 years." *Atmospheric Science Letters*, 15(1):37-43.
- Derrieux, Florence, Lionel L. Siame, Didier L. Bourlès, Rou-Fei Chen, Régis Braucher, Laetitia Léanni, Jian-Cheng Lee, Hao-Tsu Chu, and Timothy B. Byrne. 2014. "How Fast Is the Denudation of the Taiwan Mountain Belt? Perspectives from in Situ Cosmogenic ^{10}Be ." *Journal of Asian Earth Sciences* 88 (July):230-45.
- Dunne, Jeff, David Elmore, and Paul Muzikar. 1999. "Scaling Factors for the Rates of Production of Cosmogenic Nuclides for Geometric Shielding and Attenuation at Depth on Sloped Surfaces." *Geomorphology* 27:3-11.
- Fernandes, Nelson F., and William E. Dietrich. 1997. "Hillslope Evolution by Diffusive Processes: The Timescale for Equilibrium Adjustments." *Water Resources Research* 33 (6):1307-18.
- Harel, M-A, S. M. Mudd, and M. Attal. 2016. "Global Analysis of the Stream Power Law Parameters Based on Worldwide ^{10}Be Denudation Rates." *Geomorphology* 268:184-96.
- Karl, T.R., N. Nicholls, and A. Ghazi, 1999. "Clivar/GCOS/WMO workshop on indices and indicators for climate extremes workshop summary." In *Weather and Climate Extremes* (pp. 3-7). Springer, Dordrecht.
- Larson, Roger L., and John W. Ladd. 1973. "Evidence for the Opening of the South Atlantic in the Early Cretaceous." *Nature* 246 (5430):209-12.
- Lawrimore, J.H., M.J. Menne, B.E. Gleason, C.N. Williams, D.B. Wuertz, R.S. Vose, and J. Rennie, 2011. "An overview of the Global Historical Climatology Network monthly mean temperature data set, version 3." *Journal of Geophysical Research: Atmospheres*, 116(D19).
- Moon, Seulgi, C. Page Chamberlain, Kimberly Blisniuk, Nathaniel Levine, Dylan H. Rood, and George E. Hilley. 2011. "Climatic Control of Denudation in the Deglaciated Landscape of the Washington Cascades." *Nature Geoscience* 4 (7):469-73.
- Oliveira Carmo, Isabela de, and Paulo Marcos Vasconcelos. 2006. " $^{40}\text{Ar}/^{39}\text{Ar}$ Geochronology Constraints on Late Miocene Weathering Rates in Minas Gerais, Brazil." *Earth and Planetary Science Letters* 241 (1-2):80-94.
- Portenga, Eric W., and Paul R. Bierman. 2011. "Understanding Earth's Eroding Surface with ^{10}Be ." *GSA Today: A Publication of the Geological Society of America* 21 (8). geosociety.org:4-10.
- Rapp, Anita D., 2014. Alexander G. Peterson, Oliver W. Frauenfeld, Steven M. Quiring, and E. Brendan Roark. "Climatology of storm characteristics in Costa Rica using the TRMM precipitation radar." *Journal of Hydrometeorology* 15(6): 2615-2633.
- Roering, Joshua J., James W. Kirchner, and William E. Dietrich. 1999. "Evidence for Nonlinear, Diffusive Sediment Transport on Hillslopes and Implications for Landscape Morphology." *Water Resources Research* 35 (3):853-70.
- Stock, Jonathan D., and David R. Montgomery. 1999. "Geologic Constraints on Bedrock River Incision Using the Stream Power Law." *Journal of Geophysical Research. B* 104. Rocky.ess.washington.edu:4983-93.
- Zilli, Marcia T., Leila M.V. Carvalho, Brant Liebmann and Maria A. Silva Dias. 2017. "A comprehensive analysis of trends in extreme precipitation over southeastern coast of

Brazil." *International Journal of Climatology* 37: 2269-2279.

Supplementary Figures:

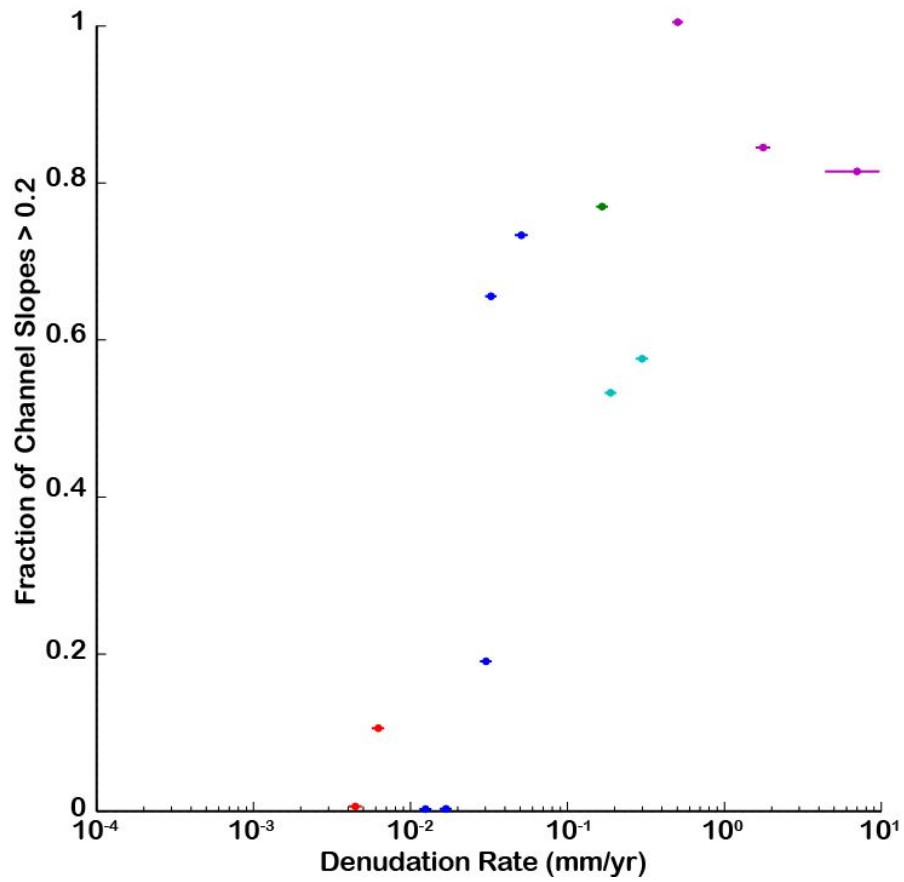


Figure S1: Denudation rate versus the fraction of basins with channel slopes > 0.2 for sampled basins. Colors represent Venezuela (red), Brazil (blue), Guatemala (cyan), Costa Rica (green) and Taiwan (purple) sampling sites.

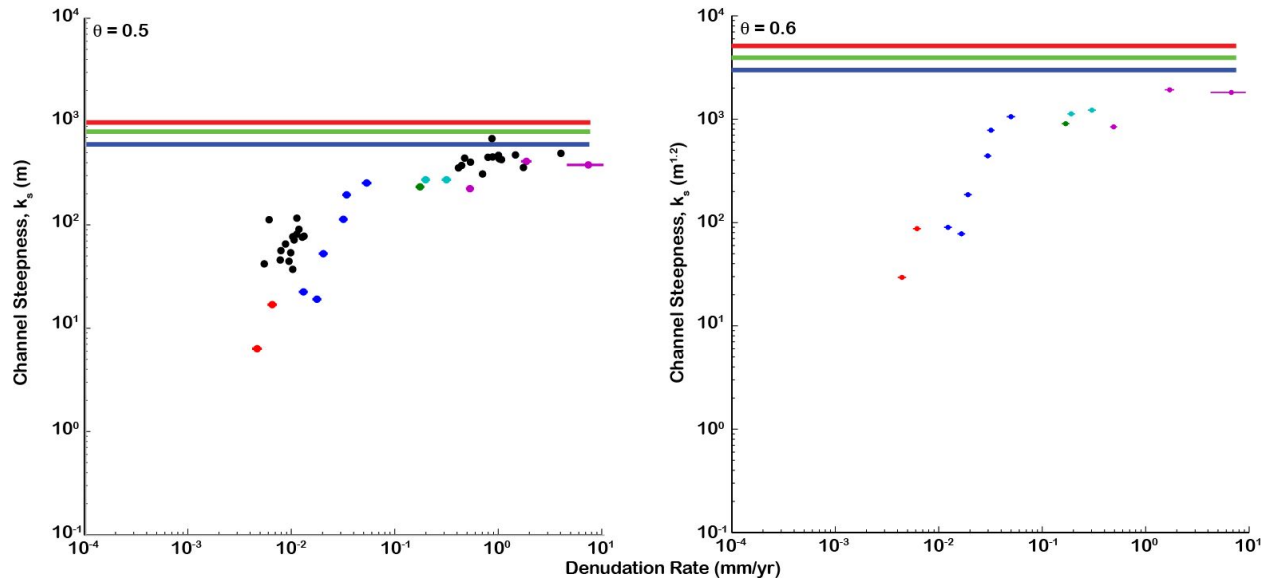


Figure S2: ^{10}Be -measured erosion rates and k_s values observed in Venezuela (red), Brazil (blue), Guatemala (cyan), Costa Rica (green) and Taiwan (purple) sampling sites for $m/n = 0.5$ (left) and $m/n = 0.6$ (right). On the left panel, horizontal blue, green, and red lines show reference steepness values of $k_s = 600, 800,$ and 1000 m, respectively. On the right panel, horizontal blue, green, and red lines show reference steepness values of $k_s = 3000, 4000,$ and 5000 $\text{m}^{1.2}$, respectively. Black dots on left panel show data from (Harel, Mudd, and Attal 2016) for comparable lithologies and mean annual precipitation range as this study. Note that the failure of global compilations to selectively and systematically sample a broad range of denudation rates prevents these studies from identifying the change in $k_s - \varepsilon$ scaling that we observe. Nonetheless, data from these global compilations are fully consistent with the change in scaling observed in this study.

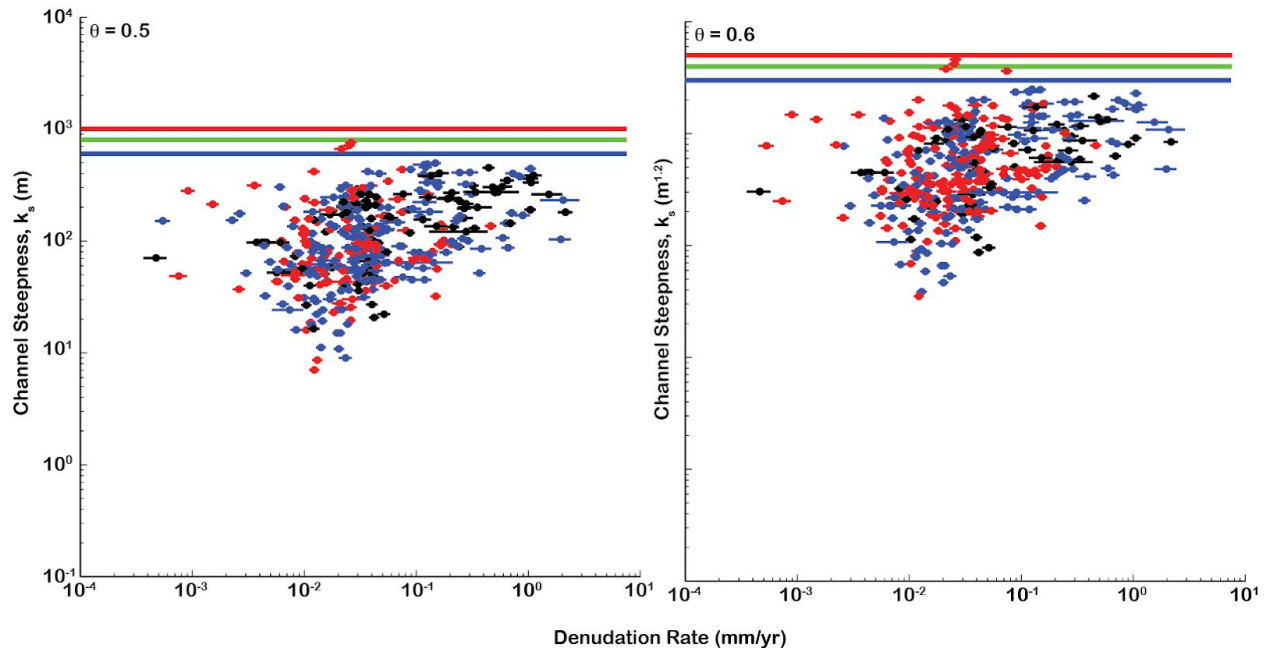


Figure S3: Global compilation of ^{10}Be -measured erosion rates (Portenga and Bierman, 2011) and k_s calculated from global elevation models using two values of concavity. Horizontal lines and fields identical to Figure 1.

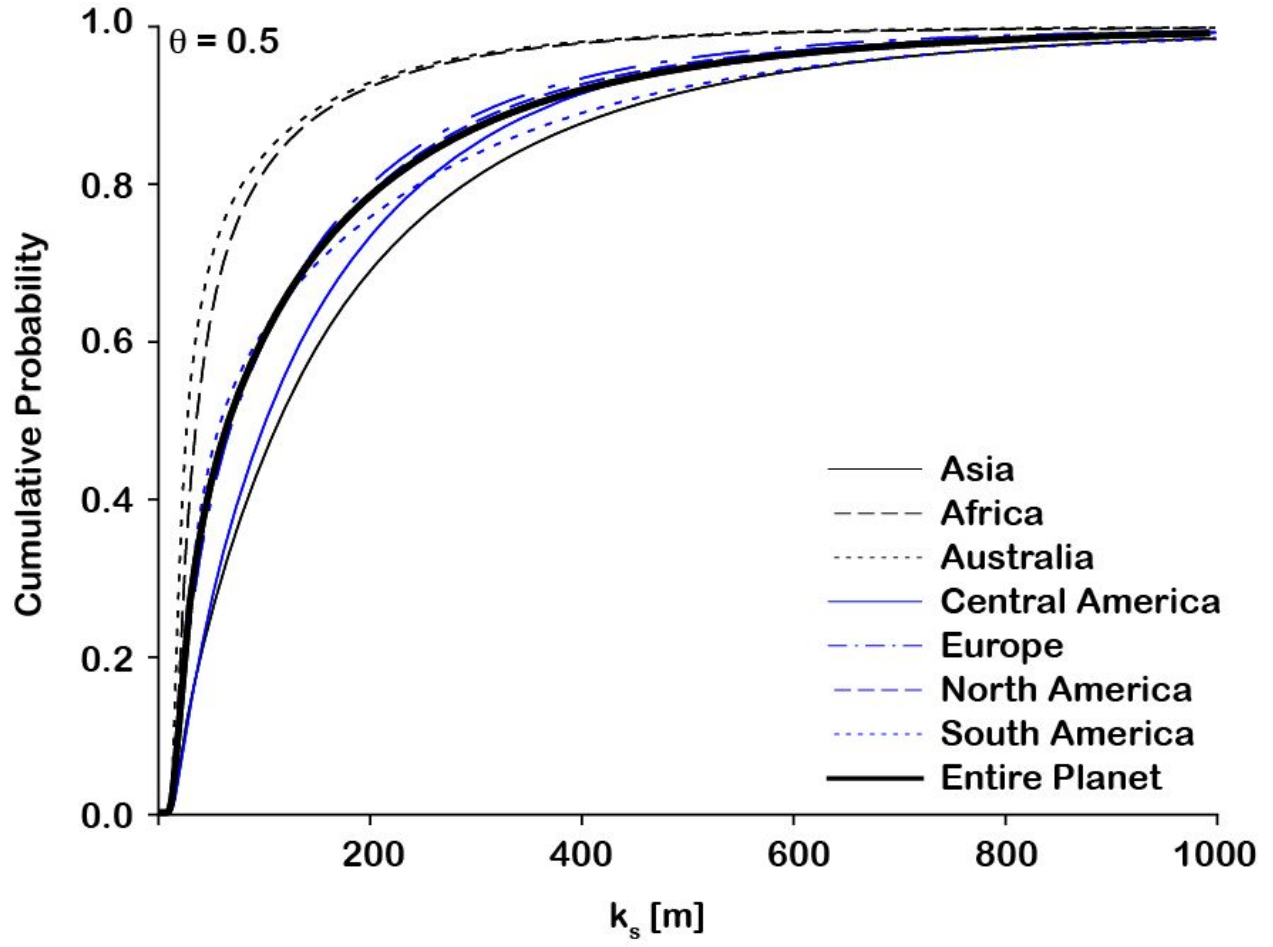


Figure S4: Cumulative density plots of k_s for $m/n=0.5$.

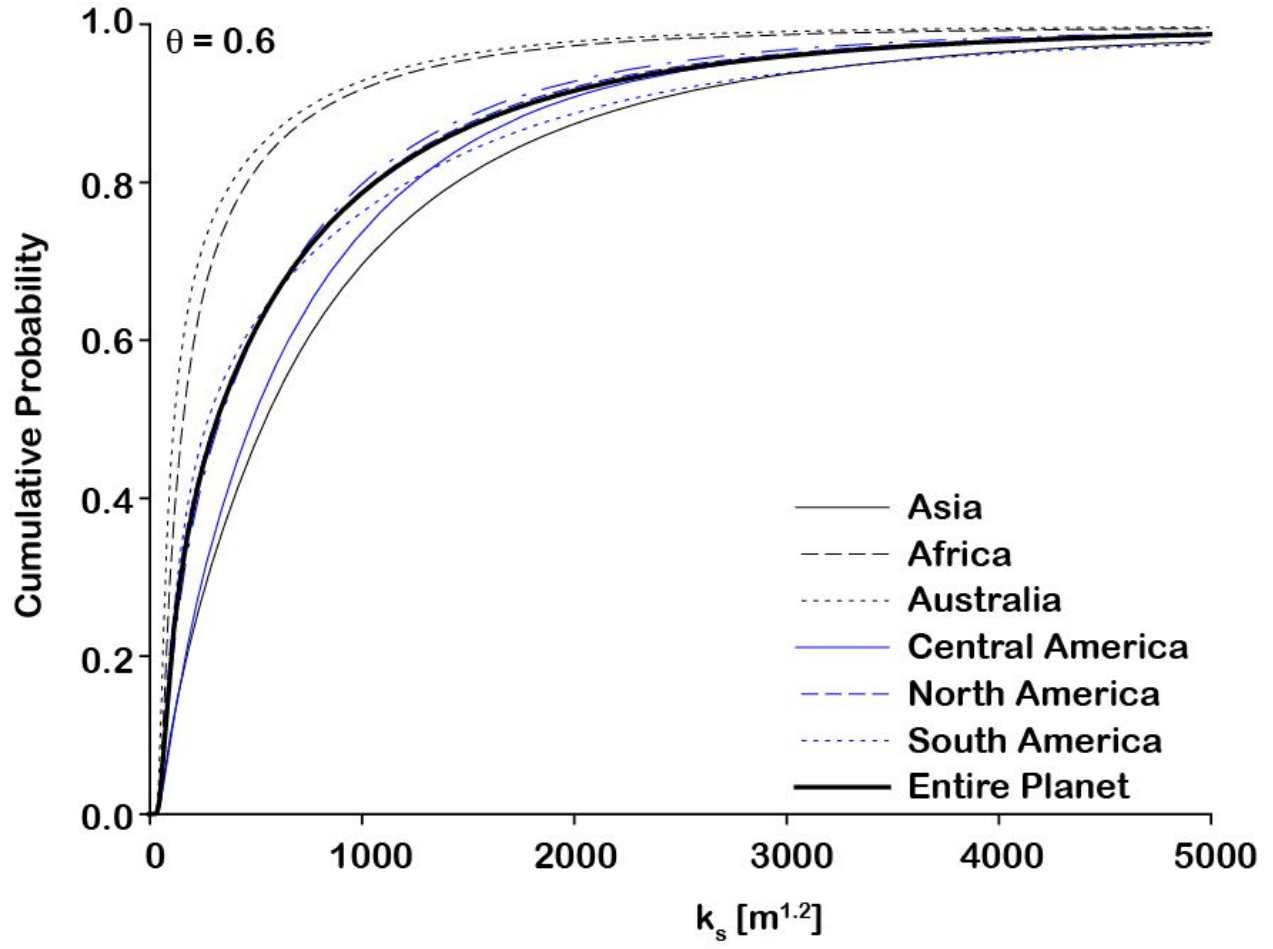


Figure S5: Cumulative density plots of k_s for $m/n=0.6$.

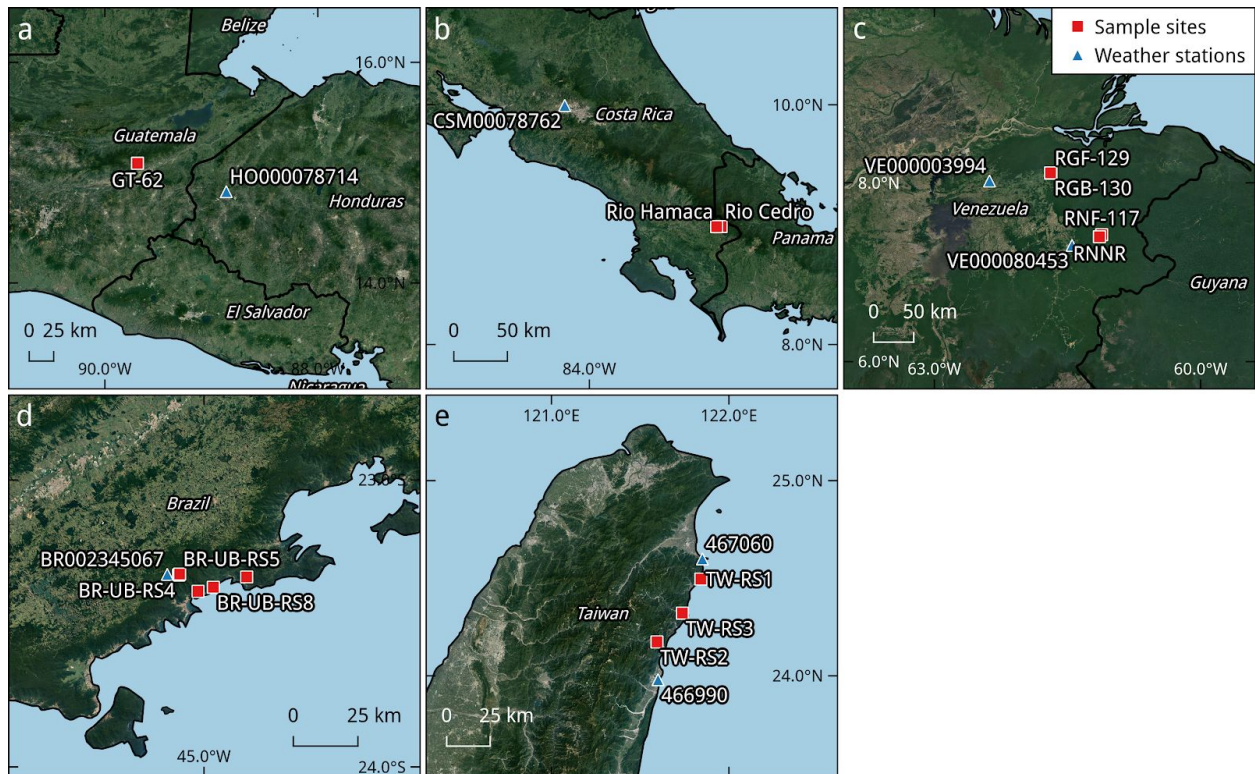


Figure S6. Map of stations (blue triangles) recording precipitation near sample sites (red squares) for cosmogenic radionuclide analysis in a) Guatemala, b) Costa Rica, c) Venezuela, d) Brazil, e) Taiwan. See Supplementary text for details of station selection. Imagery: Google, DigitalGlobe.

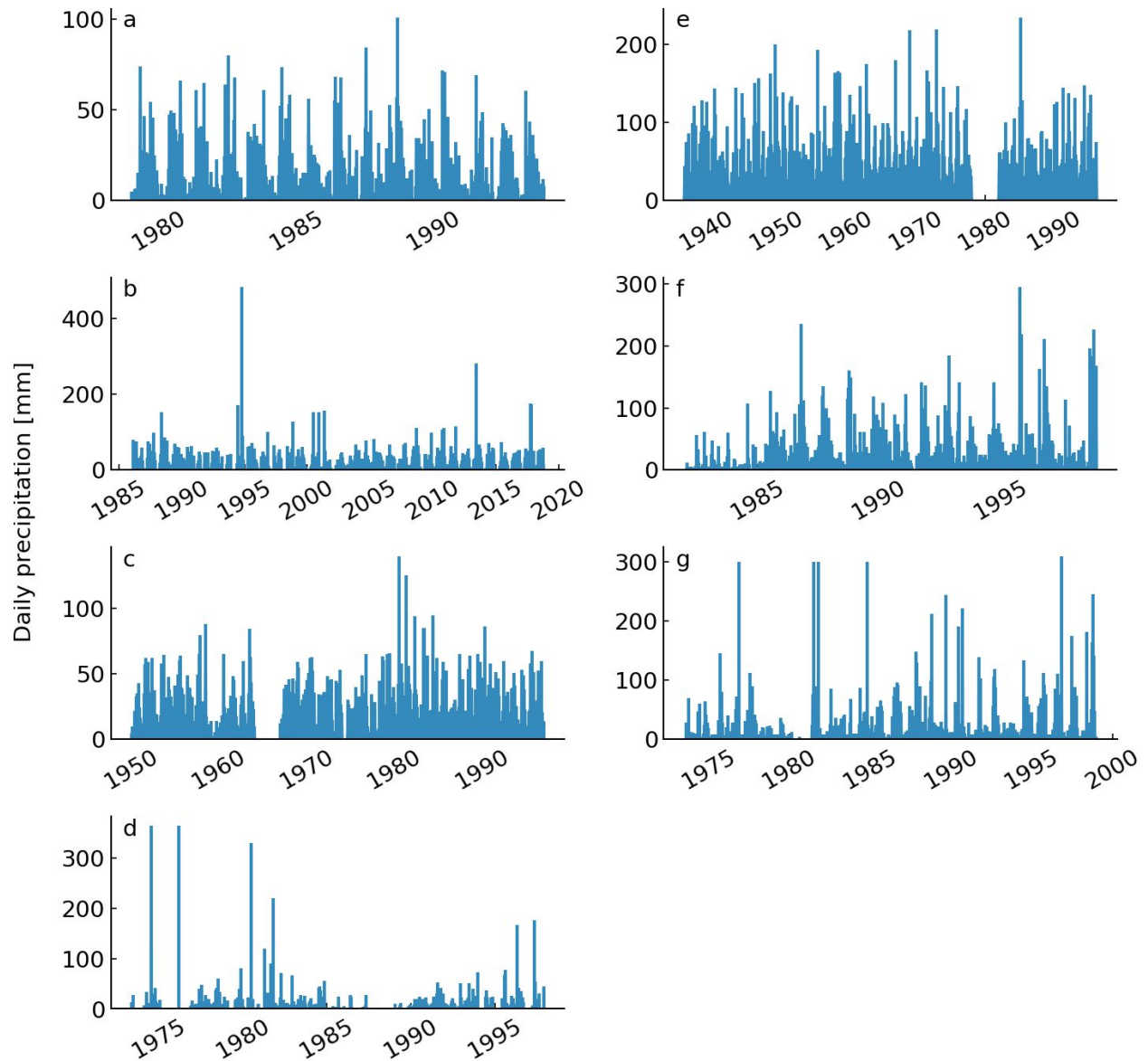


Figure S7. Precipitation records. a) Station HO000078714, Honduras, used for Guatemala site, b) Station CSM00078762, Costa Rica, c) Station VE000003994, Venezuela, d) Station VE000080453, Venezuela, e) Station BR002345067, Brazil, f) Station 467060, Taiwan, g) Station 466990, Taiwan. See Supplementary text for discussion of station selection and Table S6 for summary statistics.

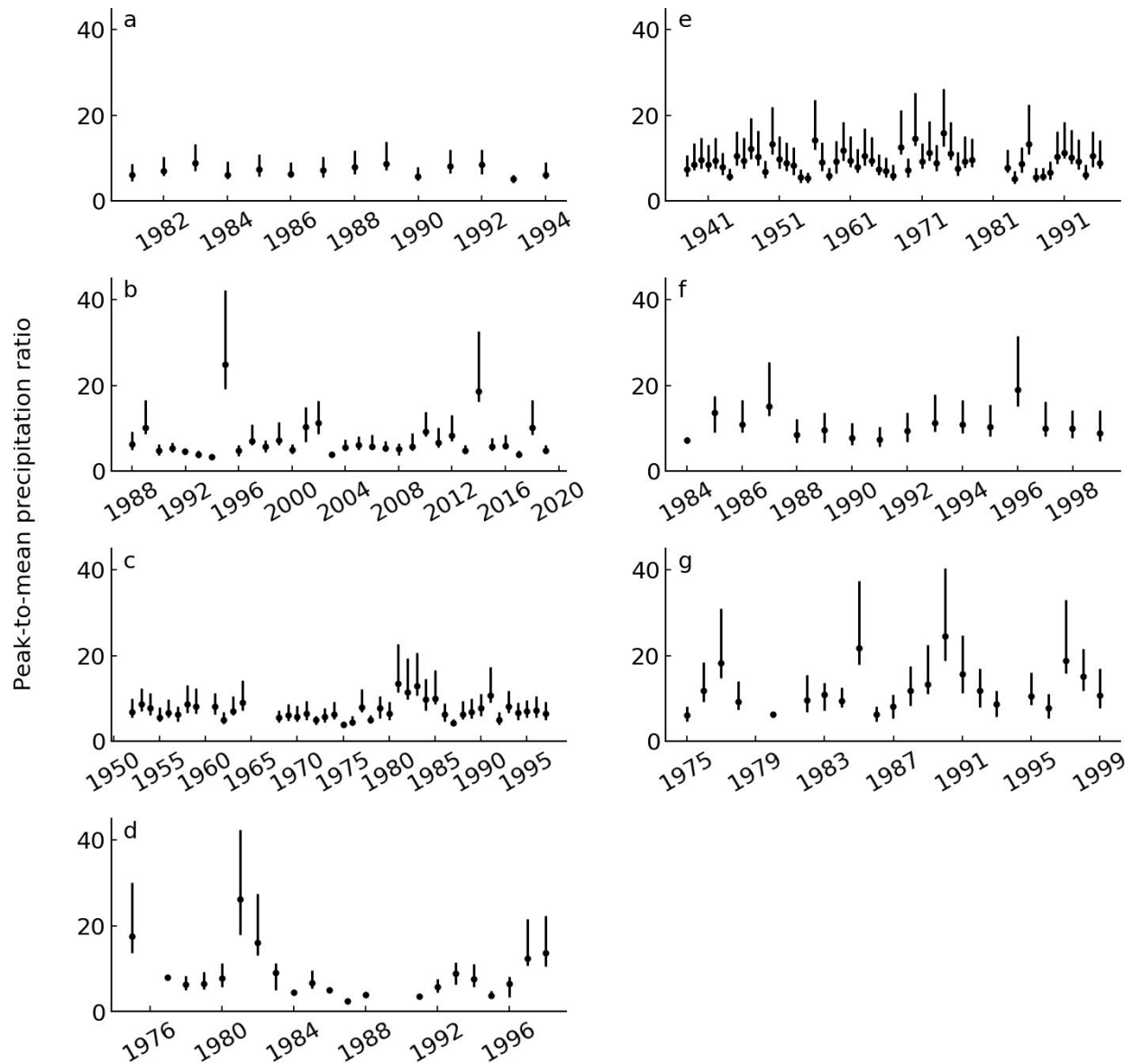


Figure S8. Frequency and relative magnitude of heavy precipitation. Each panel shows the ratios of daily precipitation to annual mean daily precipitation for days exceeding the 90th percentile intensity. Median ratios (black circles) and range of ratios (solid lines) shown for each year. See Table S6 for the peak threshold for each site. a) Station HO000078714, Honduras, b) Station CSM00078762, Costa Rica, c) Station VE000003994, Venezuela, d) Station VE000080453, Venezuela, e) Station BR002345067, Brazil, f) Station 467060, Taiwan, g) Station 466990, Taiwan.

Table S1: Parameters required to calculate erosion rates from cosmogenic radionuclide abundances measured at study sites

Sample Name	Location		Outlet Elevation (m asl)	Mean Basin Elevation (m asl)	Production Rate (atoms / g / yr)		Shielding Factor	Quartz (g)	Be Carrier (mg)	10/9 Be		10-Be		Standard	Value
	Longitude	Latitude			Spallation	Muons				Measured	Uncertainty	Concentration (atm / g)	Uncertainty (atm / g)		
<i>Venezuela</i>															
RNF-117	-61.116	7.42	159	186	3.09	0.193	1	252.5543	0.274	9.30E-12	9.85E-14	6.75E+05	7.15E+03	07KNSTD3110	2.85E-12
RNNR	-61.142	7.397	159	186	3.09	0.193	1	223.4644	0.273	9.06E-12	7.14E-14	7.39E+05	5.83E+03	07KNSTD3110	2.85E-12
RGF-129	-61.687	8.106	271	345	3.48	0.204	1	238.8594	0.273	8.00E-12	6.72E-14	6.11E+05	5.13E+03	07KNSTD3110	2.85E-12
RGB-130	-61.692	8.11	271	345	3.48	0.204	1	221.6838	0.273	6.89E-12	5.80E-14	5.67E+05	4.77E+03	07KNSTD3110	2.85E-12
<i>Brazil</i>															
BR-UB-RS1	-44.838	-23.339	29	569	5.01	0.218	0.996	199.839	0.33	1.44E-12	2.22E-14	1.59E+05	2.45E+03	07KNSTD3110	2.85E-12
BR-UB-RS4	-45.097	-23.332	977	1,035	6.93	0.254	1	200.817	0.329	4.74E-12	9.05E-14	5.20E+05	9.92E+03	07KNSTD3110	2.85E-12
BR-UB-RS5	-45.093	-23.329	974	1,036	6.93	0.254	1	206.217	0.311	3.87E-12	4.19E-14	3.91E+05	4.23E+03	07KNSTD3110	2.85E-12
BR-UB-RS6	-45.097	-23.322	987	1,075	7.13	0.257	1	196.12	0.32112	3.21E-12	9.15E-14	3.52E+05	1.00E+04	07KNSTD3110	2.85E-12
BR-UB-RS7	-45.023	-23.389	15	723	5.68	0.229	0.997	198.595	0.339	9.79E-13	4.39E-14	1.12E+05	5.01E+03	07KNSTD3110	2.85E-12
BR-UB-RS8	-44.965	-23.375	50	350	4.21	0.202	0.999	193.552	0.328	1.32E-12	2.88E-14	1.50E+05	3.27E+03	07KNSTD3110	2.85E-12
<i>Guatemala</i>															
GT-62	-89.694	15.088	1221	1,718	9.83	0.315	0.992	182.485	0.303	4.71E-13	1.19E-14	5.23E+04	1.32E+03	07KNSTD3110	2.85E-12
<i>Costa Rica</i>															
Rio Cedro	-82.888	8.985	1428	2,279	13.74	0.376	0.997	71.0764	0.332	1.18E-13	4.20E-15	3.70E+04	1.32E+03	07KNSTD3110	2.85E-12
Rio Hamaca	-82.925	8.984	1219	2,051	11.91	0.351	0.998	100.6878	0.307	2.62E-13	5.24E-15	5.33E+04	1.07E+03	07KNSTD3110	2.85E-12
<i>Taiwan</i>															
TW-RS1	121.841	24.497	7	408	4.56	0.207	0.994	358.309	0.303	1.68E-13	4.15E-15	9.52E+03	2.35E+02	07KNSTD3110	2.85E-12
TW-RS2	121.594	24.174	224	1,910	13.96	0.337	0.986	200.251	0.304	5.96E-14	3.54E-15	6.06E+03	3.60E+02	07KNSTD3110	2.85E-12
TW-RS3	121.737	24.322	37	1,467	10.5	0.293	0.989	148.651	0.309	8.70E-15	2.79E-15	1.21E+03	3.88E+02	07KNSTD3110	2.85E-12

Table S2: Erosion Rates calculated for different study sites based on data in Table S1, shown for different production-rate scaling models.

Sample Name	Lal/Stone Scaling - constant prod rate		Desilets et al.		Dunai		Lifton et al.		Lal/Stone Scaling - time varying prod rate	
	Denudation Rate (mm/yr)	1 sigma uncertainty (mm/yr)	Denudation Rate (mm/yr)	1 sigma uncertainty (mm/yr)	Denudation Rate (mm/yr)	1 sigma uncertainty (mm/yr)	Denudation Rate (mm/yr)	1 sigma uncertainty (mm/yr)	Denudation Rate (mm/yr)	1 sigma uncertainty (mm/yr)
<i>Venezuela</i>										
RNF-117	3.92E-03	3.20E-04	4.35E-03	4.60E-04	4.35E-03	4.60E-04	4.29E-03	3.90E-04	4.70E-03	3.70E-04
RNNR	3.50E-03	2.90E-04	3.90E-03	4.20E-04	3.89E-03	4.20E-04	3.84E-03	3.50E-04	4.21E-03	3.30E-04
RGF-129	4.97E-03	3.90E-04	5.56E-03	5.70E-04	5.55E-03	5.70E-04	5.50E-03	4.80E-04	5.95E-03	4.50E-04
RGB-130	5.43E-03	4.20E-04	6.06E-03	6.10E-04	6.05E-03	6.10E-04	6.00E-03	5.10E-04	6.74E-03	4.80E-04
<i>Brazil</i>										
BR-UB-RS1	3.08E-02	2.08E-03	3.04E-02	2.64E-03	3.16E-02	2.75E-03	3.12E-02	2.33E-03	3.29E-02	2.18E-03
BR-UB-RS4	1.11E-02	8.50E-04	1.17E-02	1.18E-03	1.21E-02	1.22E-03	1.21E-02	1.04E-03	1.26E-02	9.50E-04
BR-UB-RS5	1.52E-02	1.10E-03	1.58E-02	1.53E-03	1.63E-02	1.58E-03	1.63E-02	1.34E-03	1.70E-02	1.21E-03
BR-UB-RS6	1.75E-02	1.35E-03	1.81E-02	1.81E-03	1.87E-02	1.87E-03	1.87E-02	1.61E-03	1.94E-02	1.47E-03
BR-UB-RS7	4.94E-02	3.92E-03	4.82E-02	4.63E-03	5.01E-02	4.83E-03	4.93E-02	4.22E-03	5.14E-02	4.03E-03
BR-UB-RS8	2.87E-02	1.97E-03	2.81E-02	2.42E-03	2.92E-02	2.53E-03	2.87E-02	2.16E-03	3.06E-02	2.07E-03
<i>Guatemala</i>										
GT-62	1.68E-01	1.20E-02	1.64E-01	1.50E-02	1.65E-01	1.51E-02	1.63E-01	1.28E-02	1.68E-01	1.17E-02
<i>Costa Rica</i>										
Rio Cedro	3.09E-01	2.40E-02	3.08E-01	3.06E-02	3.09E-01	3.05E-02	3.03E-01	2.59E-02	3.02E-01	2.29E-02
Rio Hamaca	1.90E-01	1.35E-02	1.92E-01	1.80E-02	1.92E-01	1.79E-02	1.90E-01	1.50E-02	1.90E-01	1.32E-02
<i>Taiwan</i>										
TW-RS1	5.38E-01	3.46E-02	4.63E-01	3.47E-02	4.77E-01	3.61E-02	4.66E-01	3.13E-02	5.10E-01	3.19E-02
TW-RS2	1.94E+00	1.77E-01	1.59E+00	1.70E-01	1.63E+00	1.74E-01	1.57E+00	4.98E-02	1.79E+00	1.59E-01
TW-RS3	7.72E+00	2.81E+00	6.20E+00	2.28E+00	6.41E+00	2.35E+00	6.16E+00	2.24E+00	7.08E+00	2.57E+00

Table S3: Morphometrics for studied basins

	Basin Area (km ²)	Channel Steepness						% of Basin in which channel slope > 0.2
		$\theta = 0.4$		$\theta = 0.5$		$\theta = 0.6$		
		ks(m0.8)	R2	ks(m)	R2	ks(m1.2)	R2	
Venezuela								
RNF-117 / RNNR	208.42	1.25	0.83	6.23	0.80	29.22	0.69	0
RGF-129 / RGB-130	684.89	3.07	0.47	17.09	0.43	86.19	0.37	0.104
Brazil								
BR-UB-RS1	19.9	59.79	0.91	222.78	0.86	817.51	0.80	0.654
BR-UB-RS4	3.183	5.44	0.81	21.81	0.78	86.20	0.73	0
BR-UB-RS5	11.129	4.68	0.35	19.15	0.35	76.91	0.34	0
BR-UB-RS6	0.6	16.00	0.89	54.14	0.88	182.27	0.88	
BR-UB-RS7	35.373	53.98	0.80	242.74	0.71	1,040.64	0.57	0.731
BR-UB-RS8	10.959	25.86	0.87	108.67	0.83	439.50	0.73	0.191
Guatemala								
GT-62	5.168	57.33	0.95	228.18	0.91	885.75	0.84	0.762
Costa Rica								
Rio Cedro	43.829	60.87	0.91	275.26	0.83	1,193.69	0.71	0.576
Rio Hamaca	29.176	59.90	0.89	266.81	0.78	1,130.78	0.58	0.531
Taiwan								
TW-RS1	1.393	59.79	0.91	222.78	0.86	817.51	0.80	1
TW-RS2	523.074	80.81	0.83	414.63	0.67	1,897.95	0.32	0.842
TW-RS3	535.556	71.19	0.85	374.94	0.79	1,805.48	0.62	0.813

Table S4: Morphometrics calculated for samples in Portenga and Bierman (2011) global compilation of erosion rates in basins > 5 km²

Sample Name	Latitude (°)	Longitude (°)	Denudation Rate (mm/yr)		Area (km ²)	ks		
			Mean	Standard Deviation		$\theta = 0.4$ (m0.8)	$\theta = 0.5$ (m)	$\theta = 0.6$ (m1.2)
AO-1	7.133	80.593	1.77E-02	1.67E-03	44.81	38.5	180.2	796.2
AO-2	7.148	80.638	1.70E-02	3.04E-03	30.16	38.3	170.3	721.9
NO-1	7.188	80.631	1.89E-02	1.76E-03	62.65	32.8	145.9	614.5
NO-2	7.153	80.663	2.17E-02	1.88E-03	14.09	52.5	210.1	821.4
HUG-1	7.312	80.748	2.31E-02	2.16E-03	134.62	45.4	217.3	963.2
HUG-2	7.374	80.747	2.82E-02	4.74E-03	69.38	53.2	239.8	1018.8
MO-1	7.193	80.765	2.35E-02	2.68E-03	106.77	49.8	226.5	967.1
MO-2	7.13	80.765	6.05E-03	5.10E-04	20.97	61.2	252.9	1006.9
MO-3	7.133	80.713	2.88E-02	2.54E-03	6.11	62.1	243	935
BO-1	7.144	80.836	4.70E-02	6.22E-03	146.8	72.7	348.1	1536.1
BO-2	7.093	80.798	3.70E-02	3.82E-03	74.22	81.4	357.6	1481
UO-1	7.198	80.943	2.36E-02	2.99E-03	731.33	48.3	274.1	1393.8
UO-2	6.908	80.908	1.83E-02	4.10E-03	93.03	44.1	212.2	953.5
UO-3	6.93	80.852	3.32E-02	5.13E-03	42.05	55	256.7	1130.7
M-PER	7.261	80.595	1.51E-02	1.35E-03	1071.8	35.9	205.4	1039.4
M-HAG	7.269	80.703	2.65E-02	2.62E-03	1411.21	29.3	173.6	901.7
M-VIC	7.239	80.787	5.65E-02	6.73E-03	1900.17	30.9	186.1	975.6
M-MIN	7.211	80.981	2.74E-02	2.48E-03	3132.52	36.3	222.9	1189
N02	-15.16	-67.04	9.07E-01	1.19E-01	46.85	39.5	173.2	724.3
N04	-15.39	-67.12	1.63E-01	1.24E-02	339.6	24.6	132.8	649.3
N04	-15.39	-67.12	1.60E-01	1.28E-02	339.6	24.6	132.8	649.3
N04	-15.39	-67.12	1.68E-01	1.20E-02	339.6	24.6	132.8	649.3
N05	-15.51	-67.17	1.09E-01	1.02E-02	203.06	36.4	178.5	804.2
N06	-15.68	-67.43	1.63E-01	1.27E-02	34.05	55.7	237.1	962.4
N06	-15.68	-67.43	1.22E-01	9.22E-03	34.05	55.7	237.1	962.4
N06	-15.68	-67.43	2.44E-01	2.06E-02	34.05	55.7	237.1	962.4
S04	-19.61	-64.08	1.08E-01	8.12E-03	3929.84	45	279.7	1511.6
S04	-19.61	-64.08	8.15E-02	6.30E-03	3929.84	45	279.7	1511.6

S04	-19.61	-64.08	1.58E-01	1.15E-02	3929.84	45	279.7	1511.6
S06	-19.1	-65.3	2.66E-02	2.36E-03	1320.49	43.6	254.5	1311.5
S08	-19.52	-63.25	3.71E-01	3.78E-02	129.51	14.9	70.2	311.1
S09	-19.79	-63.23	3.92E-01	5.74E-02	154.31	19.9	94.7	419.4
S09	-19.79	-63.23	3.97E-01	4.17E-02	154.31	19.9	94.7	419.4
S09	-19.79	-63.23	3.87E-01	7.42E-02	154.31	19.9	94.7	419.4
S10	-20.01	-63.54	2.48E-01	2.15E-02	5198.58	25.7	162.3	884
S11	-19.93	-63.68	6.01E-01	7.01E-02	22.47	36.8	155.9	634.8
S12	-20.1	-63.89	2.62E-01	2.27E-02	1065.68	19.4	109.9	554
S13	-19.8	-63.94	6.70E-01	7.25E-02	64.49	22.2	103.6	455
S15	-19.17	-63.66	4.68E-01	4.39E-02	3124.85	21.5	128.8	678.3
S16	-19.2	-63.65	1.99E+00	4.00E-01	51.52	26.4	117.1	492.6
HC-Wfork	45.991	-115.337	4.65E-02	3.69E-03	16.98	22.7	100.2	420.4
HC-Efork	45.989	-115.334	4.11E-02	3.33E-03	14.82	23	99.7	412.3
TrapperCr	45.671	-115.327	3.03E-02	2.46E-03	20.54	21.9	92.8	374.5
TrapperCr	45.709	-115.344	3.05E-02	2.51E-03	97.85	30.4	145.1	641.6
UpRedRiv	45.71	-115.343	4.33E-02	3.58E-03	129.59	21.2	100.8	440.3
JohnsCreek	45.823	-115.889	5.65E-02	4.71E-03	293.06	58.6	289.4	1302.5
SForkClrwtrRiv	45.887	-116.031	4.67E-02	3.83E-03	2155.25	35.3	206.7	1050.8
LochsaRiv	46.151	-115.587	1.29E-01	1.07E-02	3055.52	38.5	244.5	1321.5
SelwayRiv	46.086	-115.514	1.08E-01	9.93E-03	4958.67	44.1	272.1	1430.5
LL1	-18.336	-69.862	2.43E-02	3.21E-03	2540	104	608	3109.8
LL1	-18.336	-69.862	2.55E-02	2.46E-03	2540	104	608	3109.8
LL1	-18.336	-69.862	2.64E-02	5.26E-03	2540	104	608	3109.8
LL1	-18.336	-69.862	2.15E-02	2.55E-03	2540	104	608	3109.8
LL2	-18.401	-70.017	2.53E-02	2.29E-03	3018	109.5	653.7	3398.4
LL3	-18.399	-70.291	2.63E-02	2.59E-03	3356	110.8	694.1	3745.9
LL3	-18.399	-70.291	2.63E-02	2.68E-03	3356	110.8	694.1	3745.9
LL3	-18.399	-70.291	2.63E-02	2.51E-03	3356	110.8	694.1	3745.9
LL4	-17.983	-69.629	1.19E-02	1.86E-03	855	35.6	186.8	886.5
LL5	-17.999	-69.631	1.24E-02	1.31E-03	1324	39.8	209.6	997.7

GSAC-1	35.611	-83.936	1.71E-02	1.35E-03	157.48	29.4	142	630.6
GSBC-1	35.749	-83.115	3.94E-02	3.02E-03	74.78	59.5	277.9	1204.3
GSBC-2	35.736	-83.13	3.82E-02	3.03E-03	65.64	53.5	245.6	1049.3
GSCA-1	35.668	-83.071	2.22E-02	1.76E-03	149.61	35.7	167.6	729.1
GSCO-1	35.505	-83.301	3.19E-02	2.46E-03	330.39	43.2	210.3	943.5
GSCO-1	35.505	-83.301	3.10E-02	2.23E-03	330.39	43.2	210.3	943.5
GSCO-1	35.505	-83.301	3.29E-02	2.69E-03	330.39	43.2	210.3	943.5
GSCO-2	35.516	-83.306	3.57E-02	2.77E-03	134.87	42.3	202.3	893.8
GSCO-3	35.521	-83.308	2.39E-02	1.83E-03	12.26	44.4	178.7	693.1
GSCO-4	35.558	-83.312	4.35E-02	3.36E-03	51.4	47.7	212.4	888.7
GSCO-5	35.567	-83.336	2.58E-02	1.99E-03	9.32	51.5	199.2	749.1
GSCS-1	35.754	-83.205	4.41E-02	3.33E-03	7.1	62.4	244.4	932.7
GSDC-1	35.464	-83.434	2.53E-02	1.95E-03	104.89	39.9	188.9	834
GSEC-1	35.487	-83.774	2.21E-02	1.76E-03	57.67	44.7	197	819.9
GSFC-1	35.47	-83.566	2.28E-02	1.82E-03	72.12	53.6	237.8	991.4
GSHC-1	35.476	-83.724	2.47E-02	1.96E-03	115.87	42.7	205.2	911.3
GSLP-1	35.738	-83.415	3.77E-02	2.94E-03	117.36	58.4	273.5	1187.8
GSLR-1	35.661	-83.707	2.95E-02	2.25E-03	155.75	40	205.1	958.4
GSLR-2	35.599	-83.514	3.84E-02	3.05E-03	7.9	46.8	179.1	668.9
GSLR-3	35.598	-83.515	5.72E-02	4.55E-03	14.64	51.7	204.7	787.3
GSLR-5	35.619	-83.54	2.97E-02	2.34E-03	29.49	39.9	168.8	680.6
GSLR-7	35.664	-83.598	3.59E-02	2.85E-03	100.43	45.9	214.7	930.3
GSNC-1	35.458	-83.528	2.25E-02	1.82E-03	46.5	47.3	216.1	924.6
GSPB-1	35.499	-83.934	2.19E-02	1.81E-03	14.96	40.3	159.8	615.6
GSRF-1	35.61	-83.255	2.33E-02	1.85E-03	36.97	31.1	137.8	578.6
GSRF-6	35.622	-83.212	2.86E-02	2.25E-03	27.28	50.7	217.2	881.8
GSRF-7	35.618	-83.208	2.34E-02	1.86E-03	7.73	41	159	602.5
GSRF-10	35.584	-83.238	2.83E-02	2.22E-03	51.84	41.9	189	795.9
GSRF-11	35.58	-83.264	2.16E-02	1.71E-03	55.89	48.7	226	984.9
GSRF-12	35.517	-83.295	2.88E-02	2.27E-03	191.6	43.3	212.8	963.9
GSTM-1	35.467	-83.878	2.33E-02	1.81E-03	39.15	49.3	213.2	874.1

GSWP-1	35.688	-83.536	3.64E-02	2.77E-03	63.65	61	281.9	1212
Wut1	47.848	8.454	7.13E-02	9.53E-03	351.56	16.3	85.4	404.6
Wut4	47.865	8.223	1.16E-01	1.75E-02	39.01	15	68.2	292.6
Wut6	47.867	8.281	4.09E-02	4.45E-03	27.7	8.7	36.9	148.7
Wut7	47.843	8.321	4.97E-02	5.93E-03	235.66	16.6	83.5	384.7
Wut9	47.88	8.163	7.64E-02	1.07E-02	16.09	12.5	55.3	232.8
JSQ1	39.946	-76.756	1.75E-02	1.34E-03	573.5	5.7	29.8	141.2
JSQ2	40.082	-76.72	1.83E-02	1.43E-03	1326.26	3.9	22.7	117.4
JSQ3	40.225	-76.898	2.52E-02	1.91E-03	558.47	6.4	37.4	194.4
JSQ4	40.255	-76.886	4.46E-02	3.59E-03	62368.9	8	59.9	366.9
JSQ5	40.323	-77.169	1.38E-02	1.09E-03	534.86	8.4	47.1	237.3
JSQ7	40.478	-77.129	2.41E-02	2.04E-03	8678.51	8.1	55	315.6
JSQ9	40.89	-77.794	1.64E-02	1.29E-03	224.2	8.3	42	195.8
JSQ10	40.943	-77.787	2.07E-02	1.60E-03	689.63	11	58	277.4
JSQ11	40.897	-78.677	2.40E-02	1.88E-03	814.45	8	43.2	210.3
JSQ12	40.216	-78.266	1.11E-02	9.00E-04	1952.58	9.4	55.9	289.4
JSQ13	40.072	-78.493	1.08E-02	8.80E-04	444.56	11.7	59.7	275.9
JS42	39.946	-76.368	2.45E-02	1.84E-03	1212.46	3.6	20.3	102.5
JS43	40.01	-76.278	1.41E-02	1.10E-03	140.75	2.6	13.2	62
JS45	39.906	-76.329	2.61E-02	1.97E-03	382.04	4.1	22.4	111.1
JSQ101	41.413	-78.197	2.70E-02	2.27E-03	704.29	13.2	71.2	347.6
JSQ103	41.592	-78.187	4.17E-02	3.81E-03	5.59	17.1	68.6	266.4
JSQ108	41.396	-78.357	1.77E-02	1.42E-03	5.38	14.4	54.9	203.7
JSQ114	41.245	-78.278	1.31E-02	1.08E-03	6.44	3.5	13.1	48.6
JSQ116	41.204	-78.039	1.53E-02	1.22E-03	6.47	10.7	42.1	161.7
JSQ119	41.274	-77.768	4.22E-02	3.54E-03	5.31	21.1	79.9	295.6
JSQ120	41.209	-77.921	2.52E-02	2.10E-03	15.11	25.7	103.3	398.6
JSQ125	41.098	-77.246	2.95E-02	2.35E-03	9.7	10.3	41.4	159.8
JSQ127	41.069	-77.308	1.06E-02	8.50E-04	5.53	5.3	20.5	78.1
JSQ131	41.075	-76.522	1.96E-02	1.76E-03	5.2	8.4	32.4	121.3
JSQ137	40.53	-77.61	1.37E-02	1.08E-03	8.64	14	57.4	229.1

JSQ153	39.829	-76.188	1.47E-02	1.17E-03	25.31	5.5	23	92.2
JSQ158	39.776	-76.493	1.14E-02	9.00E-04	7.01	5.1	20.4	79.5
JSQ159	39.806	-76.62	1.04E-02	8.50E-04	7.47	5	18.9	70.6
JSQ165	40.021	-76.359	1.23E-02	9.70E-04	104.67	2	9.2	40.2
SG0729	34.358	-117.904	8.65E-02	7.75E-03	5.31	37.9	148.3	564.3
SH-01	38.571	-78.287	3.61E-02	2.83E-03	39.49	45.1	193.3	786.4
SH-01A	38.571	-78.287	3.05E-02	2.30E-03	39.49	45.1	193.3	786.4
SH-01B	38.571	-78.287	3.11E-02	2.49E-03	39.49	45.1	193.3	786.4
SH-01C	38.571	-78.287	3.50E-02	2.98E-03	39.49	45.1	193.3	786.4
SH-01D	38.571	-78.287	4.79E-02	3.54E-03	39.49	45.1	193.3	786.4
SH-03	38.362	-78.654	7.03E-03	1.15E-03	9.43	18.6	74.7	289.8
SH-03A	38.362	-78.654	8.89E-03	1.39E-03	9.43	18.6	74.7	289.8
SH-03B	38.362	-78.654	6.73E-03	1.17E-03	9.43	18.6	74.7	289.8
SH-03C	38.362	-78.654	5.66E-03	9.50E-04	9.43	18.6	74.7	289.8
SH-03D	38.362	-78.654	6.83E-03	1.10E-03	9.43	18.6	74.7	289.8
SH-04	38.199	-78.794	4.58E-03	7.90E-04	12.71	27.4	112.7	446.1
SH-04A	38.199	-78.794	4.18E-03	7.20E-04	12.71	27.4	112.7	446.1
SH-04B	38.199	-78.794	3.75E-03	6.40E-04	12.71	27.4	112.7	446.1
SH-04C	38.199	-78.794	4.26E-03	7.40E-04	12.71	27.4	112.7	446.1
SH-04D	38.199	-78.794	6.13E-03	1.07E-03	12.71	27.4	112.7	446.1
SH-11	38.653	-78.245	1.56E-02	1.19E-03	24.31	32.1	138.4	565.3
SH-12	38.615	-78.257	1.42E-02	1.11E-03	14.19	32.4	136.8	554.1
SH-15	38.521	-78.29	1.19E-02	9.10E-04	5.97	27.6	109.9	424.1
SH-16	38.542	-78.352	2.13E-02	1.61E-03	13.8	55.1	221.8	861
SH-17	38.78	-78.366	4.37E-03	3.70E-04	9.28	29.5	115.8	442.7
SH-19	38.471	-78.498	1.23E-02	9.60E-04	11.49	36.4	149.9	592.7
SH-21	38.645	-78.369	1.33E-02	1.02E-03	5.65	34.6	137.1	528
SH-23	38.869	-78.178	1.62E-02	1.22E-03	18.73	26.5	106.4	411.3
SH-25	38.148	-78.749	7.92E-03	7.30E-04	25.22	33.5	145.7	601.7
SH-28	38.099	-78.804	5.63E-03	4.60E-04	5.7	22.6	86.1	320.6
SH-31	38.16	-78.803	7.03E-03	5.70E-04	8.47	25.7	101.6	390.3

SH-38	38.257	-78.769	8.27E-03	6.60E-04	15.12	29.1	115.9	446.4
SH-48	38.838	-78.106	1.31E-02	9.90E-04	16.85	26.8	106.6	409.7
SH-49	38.927	-78.176	3.02E-03	2.70E-04	10.88	13	52.9	208.9
SH-52	38.811	-78.234	1.13E-02	8.80E-04	22.91	31.6	131.2	524.1
SH-56	38.532	-78.603	6.59E-03	5.40E-04	3305.62	10.6	65	343.9
NFC	39.361	-123.736	1.65E-01	1.47E-02	5.02	13.2	51.9	198
COY	41.117	-123.913	2.70E-01	3.24E-02	20.39	52.5	214.3	837.5
LLM	41.322	-124.02	2.09E-01	2.12E-02	8.37	28.5	111.5	423.6
ORK	41.289	-124.06	6.45E-01	6.39E-02	720.45	27	155.6	786.9
PAN	41.088	-123.908	3.36E-01	3.01E-02	15.52	37.6	152.3	591.9
N4-N-SC	30.487	34.938	1.49E-02	1.41E-03	16.25	15.6	65.9	265.4
N4-R-SD	30.6	34.937	3.00E-02	2.52E-03	214.45	13.8	68.9	313.6
N4-NR-SD	30.591	34.943	3.20E-02	3.68E-03	343.48	13.9	70	321.3
N1-SD	30.662	35.107	4.31E-02	3.68E-03	797.63	19.5	107.7	532
TC-20	-12.459	133.289	5.19E-02	5.62E-03	11.93	6.7	26.9	104.4
TC-21	-12.455	133.288	4.04E-02	3.82E-03	12.48	7.4	30	117.7
TC-22/23	-12.453	133.27	1.01E-02	1.75E-03	387.33	9.5	49.7	236.5
TC-22	-12.453	133.27	1.24E-02	2.34E-03	387.33	9.5	49.7	236.5
TC-23	-12.453	133.27	8.25E-03	1.36E-03	387.33	9.5	49.7	236.5
MD-110	-23.591	132.536	7.50E-04	1.20E-04	212.44	9.4	46.9	216.1
MD-119	-23.699	132.355	7.70E-03	1.47E-03	10	7	28.5	111.9
MD-119	-23.699	132.355	9.55E-03	1.12E-03	10	7	28.5	111.9
MD-119	-23.699	132.355	7.40E-03	2.14E-03	10	7	28.5	111.9
Piu10	-4.945	-79.996	1.28E-01	1.32E-02	93.88	89.7	396.3	1665.7
Piu9	-5.018	-80.054	1.26E-01	1.35E-02	153.99	96.5	471.1	2122
Piu8	-5.086	-80.132	1.22E-01	1.36E-02	186.69	83.5	431.2	2030.2
Piu6	-5.104	-80.158	8.95E-02	7.33E-03	192.97	77.6	408.5	1959.3
2_10	-5.061	-79.875	2.47E-01	3.36E-02	51.16	88	381.4	1576.2
2_12	-5.114	-79.895	1.19E-01	2.25E-02	136.46	97.5	449.2	1931.7
Piu3	-5.138	-79.911	1.49E-01	1.42E-02	147.54	100.9	479.9	2114.6
Piu4	-5.211	-80.016	3.93E-02	4.79E-03	2944.99	52.3	302.1	1532.3

Piu7	-5.115	-80.173	6.84E-02	1.05E-02	4660.91	38.2	227	1176.4
2_16	-4.938	-80.344	1.66E-02	2.81E-03	6388.59	30.1	185	980.3
Piu2	-5.162	-80.615	2.44E-02	2.47E-03	7486.71	23.5	152.8	843.4
2_9	-5.06	-79.876	1.17E-01	1.20E-02	43.93	90.4	399.5	1671.4
2_11	-5.104	-79.876	3.23E-02	3.09E-03	7.37	76	299.6	1152.3
NAM-08	-23.318	16.449	4.48E-03	4.00E-04	65.63	6	27.8	121.1
NAM-09	-23.248	16.3	1.46E-02	1.22E-03	14.51	24.2	98.9	389.3
NAM-16	-23.303	15.773	8.25E-03	6.70E-04	6556.92	22.1	137.4	734.2
NAM-46	-21.915	15.571	6.51E-03	5.60E-04	4793.63	14	84.8	449.6
NAM-52	-22.086	14.269	1.51E-03	1.60E-04	11490	28.7	194.9	1113.6
NAM-57	-21.166	13.667	6.79E-03	6.00E-04	29337.7	25.7	182.5	1074.6
wp-8	-31.557	138.576	4.94E-03	4.70E-04	8.6	7.3	29.3	113.9
wp-9	-31.545	138.591	2.60E-03	2.60E-04	72.47	12.2	55.9	242.1
tc-1	-23.568	134.437	1.87E-02	1.95E-03	432.29	10.7	57.4	277.6
tc-2	-23.524	134.392	2.03E-02	2.21E-03	433.67	10.2	52	242.9
tc-3	-23.567	134.433	1.46E-02	1.77E-03	473.35	11	58.7	284.5
LUI34	30.497	-98.82	3.58E-02	4.30E-03	28.95	9.8	41.7	169.9
LUI35	30.554	-98.701	2.25E-02	2.47E-03	392.45	9.3	48	224.9
RP-1	34.41	-106.853	4.85E-02	3.95E-03	16146.4	19.1	125.6	692.3
RP-2	34.545	-106.884	3.69E-02	3.00E-03	15436.9	19.1	124.7	683.4
RP-3	34.575	-106.89	1.61E-02	1.34E-03	465.61	15.1	80.2	388.5
RP-4	34.584	-106.885	6.89E-02	5.65E-03	14939.3	19.1	124.5	683
RP-5	34.869	-107.022	9.27E-02	7.50E-03	14218.1	18.8	119.3	642.1
RP-6	34.887	-107.033	7.31E-02	6.03E-03	7117.05	16.8	107.8	583.9
RP-7	34.892	-107.028	1.13E-01	9.50E-03	7077.01	16.8	107.8	583.9
RP-8A	35.039	-107.339	5.74E-02	4.67E-03	5102.73	18.5	112.4	587.1
RP-9	35.093	-107.323	1.45E-01	1.39E-02	309.83	31.7	159.4	736.9
RP-14A	35.355	-108.011	5.09E-02	4.16E-03	744.17	10.4	54	253
RP-14B	35.35	-108.01	5.80E-02	4.72E-03	746.64	10.4	54	253
RP-18	35.342	-108.214	6.77E-03	6.00E-04	190.57	12.9	63.7	289.4
RP-19	35.034	-106.942	1.32E-01	1.08E-02	6594.53	16.8	105.6	565.1

RP-20	35.336	-107.035	1.23E-01	1.00E-02	302.37	22	114	533.6
RP-21	35.348	-107.043	1.24E-01	1.11E-02	5338.92	16.2	98.7	518.3
RP-22	35.571	-107.168	1.22E-01	1.03E-02	4736.18	15.1	87.6	445.8
RP-23	35.599	-107.18	1.62E-01	1.46E-02	1116.97	17.9	104.5	534.4
RP-24	35.925	-106.986	2.37E-01	2.21E-02	538.03	18.2	92	423.7
RP-25	35.95	-107.007	1.49E-01	1.32E-02	170.1	8.7	42.2	188.4
RP-26	35.956	-106.994	3.65E-01	3.54E-02	358.1	22.1	111.7	515
RP-27	35.593	-107.192	1.18E-01	9.95E-03	3562.52	13.5	77.1	387.6
RP-28	35.642	-107.241	1.54E-01	1.31E-02	1290.98	10.3	57.4	284.6
RP-29	35.627	-107.24	7.46E-02	6.17E-03	2218.48	14.9	84.4	421.6
RP-30	35.81	-107.255	2.00E-01	1.68E-02	776.77	7.6	39.1	182.7
RP-31	35.824	-107.258	2.56E-01	2.30E-02	301.27	7.9	39.1	176.8
RP-32	35.82	-107.271	1.69E-01	1.47E-02	471.11	7.3	37.2	173.2
RP-33	35.657	-107.392	6.49E-02	5.41E-03	569.82	8.8	46	217.2
RP-34	35.655	-107.392	7.24E-02	6.10E-03	1328.44	14.1	77.8	382.5
RP-35	35.588	-107.486	4.85E-02	4.03E-03	464.54	21.8	114.1	541
RP-36	35.577	-107.521	3.91E-02	3.28E-03	207.22	11.1	55.5	253
RP-37	35.58	-107.521	6.05E-02	5.07E-03	511.21	9.2	48.6	233.3
RP-39	35.34	-107.793	3.89E-02	3.30E-03	251.4	22.8	109.7	486.1
RP-40	35.338	-107.795	3.05E-02	2.66E-03	197.49	9.6	45.7	202.3
RP-41	35.336	-107.796	2.86E-02	2.53E-03	449.27	16.6	80	355.9
RP-42	35.434	-108.042	1.01E-01	8.50E-03	323.73	11.5	57.8	266.4
O128o	-21.455	15.075	9.77E-03	7.60E-04	7971.2	17.1	106.2	565.9
O149l	-21.289	15.237	8.46E-03	6.70E-04	174.08	9.3	45.4	206.3
O149o	-21.342	15.202	9.92E-03	7.80E-04	7374.15	16.9	103.1	544.1
O171o	-21.348	15.406	1.02E-02	7.90E-04	6570.88	15.3	91.4	476.8
O195o	-21.41	15.639	1.06E-02	8.30E-04	3798.01	13.9	83.2	434.4
O269o	-21.304	16.217	8.63E-03	6.80E-04	1090.92	9.5	51.8	254.6
O269ot	-21.306	16.216	1.13E-02	8.90E-04	227.91	10	51.8	245.1
O291n	-21.166	16.348	8.32E-03	6.70E-04	395.81	8.6	44.9	216.1
O299s	-21.173	16.402	8.86E-03	7.20E-04	148.21	8.1	38.9	176.2

S160t	-22.519	15.858	1.23E-02	9.40E-04	684.03	16.5	83.6	384
S184s	-22.389	15.835	1.10E-02	8.60E-04	14052.5	21.6	139.9	767.9
S216s	-22.352	16.144	1.30E-02	1.00E-03	11342	20.2	128.8	701.5
S259s	-22.263	16.43	1.02E-02	8.60E-04	8831.79	17.2	106.3	567.5
S279sn	-22.154	16.577	1.09E-02	8.50E-04	438.5	10.2	53.1	253
S330o	-22.238	17.023	9.70E-03	7.80E-04	307.62	21.1	110.7	529.4
S333s	-22.085	16.881	8.63E-03	7.20E-04	3769.2	11.7	67.8	345.1
S337o	-22.038	16.921	8.11E-03	1.80E-03	597.53	8.1	43	208.5
S337s	-22.038	16.922	1.17E-02	9.40E-04	2977.63	11.5	66.8	341.1
S397s	-21.848	17.295	9.61E-03	7.70E-04	910.68	10.3	54.9	264
S6s	-22.682	14.531	1.01E-02	7.90E-04	29292.4	30.3	213.2	1238.4
SkU	-22.008	15.588	6.25E-03	5.10E-04	6087.1	15	90.2	474.3
QLD1	-16.822	145.637	1.96E-02	1.34E-03	8.02	9.7	39.4	155
QLD2	-16.822	145.637	2.11E-02	1.53E-03	8.03	9.7	39.4	155
QLD3	-16.963	145.677	4.18E-02	2.86E-03	55.66	28.5	127.7	543.8
QLD5	-16.852	145.648	1.72E-02	1.34E-03	1991.83	18.7	111.9	590.1
QLD6	-16.873	145.671	6.49E-03	5.00E-04	10.82	46	183.8	714.8
QLD7	-16.907	145.561	2.14E-02	1.46E-03	76.59	10.6	49.8	219.4
QLD8	-16.899	145.551	2.05E-02	1.41E-03	142.58	16.4	81	370.4
QLD9	-16.824	145.512	1.52E-02	1.06E-03	287.62	11.4	59.4	282
QLD9	-16.824	145.512	1.48E-02	1.03E-03	287.62	11.4	59.4	282
QLD9	-16.824	145.512	1.52E-02	1.07E-03	287.62	11.4	59.4	282
QLD9	-16.824	145.512	1.50E-02	1.04E-03	287.62	11.4	59.4	282
QLD10	-16.801	145.617	1.53E-02	1.11E-03	1941.88	11.7	68.4	352.7
MHC-8	34.129	-116.976	3.42E-01	5.35E-02	8.04	75.5	296.2	1131.9
MHC-13	34.128	-116.985	5.95E-01	1.15E-01	8.76	79.4	317	1229.8
MHC-14	34.133	-116.988	2.82E-01	3.89E-02	9.36	79.4	317	1229.8
MHC-15	34.129	-116.989	2.80E-01	3.87E-02	18.2	75.1	304.8	1194.1
CAY	18.158	-65.959	7.01E-02	1.71E-02	32.37	13.6	60.7	257.6
CAY 0.063	18.158	-65.959	4.19E-02	6.21E-03	32.37	13.6	60.7	257.6
CAY 0.125	18.158	-65.959	4.32E-02	5.96E-03	32.37	13.6	60.7	257.6

CAY 0.25	18.158	-65.959	4.34E-02	7.08E-03	32.37	13.6	60.7	257.6
CAY 0.50	18.158	-65.959	5.54E-02	7.94E-03	32.37	13.6	60.7	257.6
CAY 1.0	18.158	-65.959	9.16E-02	1.22E-02	32.37	13.6	60.7	257.6
CAY 2.0	18.158	-65.959	7.11E-02	1.53E-02	32.37	13.6	60.7	257.6
CAY 4.0	18.158	-65.959	1.44E-01	6.51E-02	32.37	13.6	60.7	257.6
2	29.78	116.245	1.58E-01	1.69E-02	1695910	26.5	250.9	1760.5
3	28.262	115.846	3.09E-02	4.05E-03	74441.8	7.2	55.8	351
4	30.522	112.888	6.71E-02	6.08E-03	144396	15.9	130.1	838.4
6	28.357	112.881	4.60E-02	4.45E-03	99117.7	7.6	59.8	378.3
7	29.047	111.552	4.49E-02	4.55E-03	89992.3	11.8	95.1	621.6
8	29.779	112.47	1.63E-01	1.78E-02	1058380	33.5	329.3	2428.6
10	29.876	106.403	6.17E-02	6.41E-03	145891	22.7	183.8	1198.7
10	29.876	106.403	5.21E-02	5.69E-03	145891	22.7	183.8	1198.7
10	29.876	106.403	7.53E-02	7.29E-03	145891	22.7	183.8	1198.7
11	29.361	106.423	7.51E-02	6.86E-03	730372	41.3	399.9	2926
YPG 2	33.04	-114.522	4.30E-02	5.10E-03	186.71	14	69.1	314.1
YPG 2A	33.04	-114.522	4.37E-02	4.58E-03	186.71	14	69.1	314.1
YPG 2B	33.04	-114.522	3.43E-02	3.44E-03	186.71	14	69.1	314.1
YPG 2C	33.04	-114.522	4.50E-02	4.66E-03	186.71	14	69.1	314.1
YPG 2D	33.04	-114.522	4.10E-02	4.60E-03	186.71	14	69.1	314.1
YPG 2E	33.04	-114.522	4.94E-02	7.38E-03	186.71	14	69.1	314.1
YPG 2F	33.04	-114.522	4.47E-02	5.96E-03	186.71	14	69.1	314.1
YPG 3A	33.098	-114.534	4.10E-02	3.71E-03	28.74	11	45.9	184.4
YPG 4	33.089	-114.531	3.80E-02	4.26E-03	40.38	10.4	45.1	187.4
YPG 4A	33.089	-114.531	4.12E-02	4.80E-03	40.38	10.4	45.1	187.4
YPG 4B	33.089	-114.531	3.48E-02	3.71E-03	40.38	10.4	45.1	187.4
YPG 5A	33.089	-114.524	3.62E-02	3.15E-03	120.08	12.4	59.5	266.2
YPG 17A	33.117	-114.505	3.18E-02	2.51E-03	102.62	11.6	54.3	238.3
YPG 18A	33.146	-114.499	3.08E-02	2.39E-03	29.08	8.5	37	153.8
YPG 19	33.155	-114.516	2.71E-02	2.30E-03	59.52	12.2	55.9	242.2
YPG 19A	33.155	-114.516	2.81E-02	2.49E-03	59.52	12.2	55.9	242.2

YPG 19B	33.155	-114.516	2.56E-02	2.15E-03	59.52	12.2	55.9	242.2
YPG 19C	33.155	-114.516	2.39E-02	1.98E-03	59.52	12.2	55.9	242.2
YPG 19F	33.155	-114.516	3.07E-02	2.59E-03	59.52	12.2	55.9	242.2
YPG 21A	33.177	-114.517	2.27E-02	1.78E-03	34.6	12.4	56.3	242.8
YPG 28	33.207	-114.519	2.36E-02	1.95E-03	22.37	12	51.7	212.8
2004-6A	-19.005	47.125	1.18E-02	9.70E-04	208.64	20.9	109.3	523.9
2004-9A	-18.95	47.526	5.79E-03	4.90E-04	1585.92	8.7	51.6	270.5
2004-2A	-18.945	46.823	1.60E-02	1.31E-03	133.54	9.8	48.5	221.6
2005-3C	-17.55	48.208	1.30E-02	1.02E-03	5.25	6	23.3	89.1
2005-7	-17.628	48.204	2.23E-02	1.64E-03	57.5	10.9	49.5	211.4
1	44	12	3.54E-01	4.48E-02	10.17	25.6	99	370.5
1	37.967	15.381	1.06E+00	9.83E-02	26.23	47.2	209.8	879.7
2	38.003	15.405	1.55E+00	4.48E-01	49.09	53.6	240.1	1008.1
3	37.943	15.758	2.19E+00	2.74E-01	25.98	41.6	178.9	728.9
4	37.948	15.962	1.50E+00	2.98E-01	20.39	52.1	219.5	877.4
4	37.948	15.962	1.08E+00	1.39E-01	20.39	52.1	219.5	877.4
4	37.948	15.962	2.09E+00	7.60E-01	20.39	52.1	219.5	877.4
5	38.005	16.084	7.20E-01	6.39E-02	40.95	42.8	182.7	740.2
SGB1	34.304	-118.156	1.22E-01	2.69E-02	174.7	45.7	217.9	960.8
SGB2	34.304	-118.108	1.33E-01	3.69E-02	101.91	39.8	185.2	801.5
SGB3	34.31	-118.121	9.36E-02	1.54E-02	106.52	40.9	193.7	851.4
SGB4	34.276	-118.026	3.74E-02	9.71E-03	5.68	27.2	109	425.8
SGB5	34.328	-118.12	1.53E-01	3.26E-02	10.18	38.6	157.7	622.4
SGB6	34.327	-118.25	2.82E-01	1.48E-01	11.08	60.8	239.5	912.9
SGB9	34.301	-118.255	5.11E-01	3.87E-02	17.34	63.7	268.7	1083.2
SGB11	34.295	-117.739	8.54E-01	7.27E-02	82.85	83.7	378	1601.7
SGB12	34.24	-117.761	1.06E+00	9.71E-02	148.98	87.4	419.9	1862.3
SGB13	34.295	-117.742	4.49E-01	4.38E-02	35.03	89.5	394	1645.2
SG137	34.271	-117.889	6.57E-01	7.68E-02	47.02	76.9	335.5	1381.7
SG138	34.27	-117.891	4.87E-01	8.08E-02	17.94	73.8	306	1216.9
SG141	34.252	-117.973	3.22E-01	3.38E-02	43.47	65.3	286.3	1183.4

SG157	34.304	-117.73	1.13E+00	1.75E-01	25.49	89	379.5	1538.5
SG158	34.304	-117.732	1.08E+00	1.52E-01	53.26	77.3	346.3	1457.3
SG159	34.294	-117.741	7.38E-01	9.00E-02	117.93	85.6	389.1	1658.2
SG161	34.301	-117.761	1.04E+00	1.68E-01	11.57	76.9	315.7	1245.1
SG162	34.163	-117.635	3.04E-01	4.78E-02	28.04	95.8	408.8	1660.6
SG206	34.23	-117.791	3.55E-01	1.11E-01	5.41	69.1	265.9	996.9
Wut10	47.939	8.201	4.38E-02	5.71E-03	19.75	17.2	70.8	279.1
Wut12	47.869	8.262	5.26E-02	6.41E-03	126.98	14.2	70.2	319.7
Don1	47.983	8.242	3.41E-02	3.98E-03	8.65	12.4	48.8	186.1
Don3	47.948	8.367	1.12E-02	1.12E-03	5.12	10.6	41.1	155.4
CCC	9.36	-79.325	1.55E-01	1.28E-02	61.29	15.1	68.6	294.4
CChC	9.267	-79.506	2.07E-01	1.86E-02	406.6	18.9	100.8	489.3
CHAG-17	9.296	-79.411	1.41E-01	1.25E-02	176.02	17.2	87	407.5
CHAG-19	9.269	-79.505	1.64E-01	1.68E-02	364.19	19	101	488.8
Chico	9.271	-79.507	1.87E-01	2.05E-02	40.91	20.3	96.1	429.5
CHM-1	9.36	-79.321	1.26E-01	9.69E-03	34.9	17.8	79.4	337
CLA	9.244	-79.531	1.78E-01	1.54E-02	461.16	19.9	107	524
CPC	9.294	-79.416	1.67E-01	1.44E-02	269.49	19.3	97.7	457.3
CTOM	9.365	-79.323	1.51E-01	1.27E-02	24.11	14	61	253.9
PIED	9.293	-79.411	1.75E-01	1.42E-02	92.88	28.1	132.6	585.3
Y3	39.221	99.621	1.16E-01	1.79E-02	13.13	37	158.3	652.2
Y8	39.119	99.877	2.68E-01	4.90E-02	8.7	40.2	161	623.3
Y9	39.117	99.925	5.44E-01	2.72E-01	30.51	60.2	257.3	1043.8
L2	39.185	100.381	3.36E-02	4.76E-03	7.62	18.7	72.3	272.4
L8	39.053	100.703	1.25E-01	1.72E-02	47.42	53	235.1	984.5
L9	38.957	100.805	2.10E-01	3.04E-02	15.79	70.3	288.5	1135.5
L10*	38.945	100.84	1.29E-01	2.01E-02	8.06	62.3	246.1	947.8
ASOI-SD	-24.093	-70.269	9.10E-04	1.10E-04	532.56	44.7	228.4	1059.1
ADBA-5SD	-23.4	-69.463	2.26E-03	2.30E-04	763.46	26.8	137.8	645.9
ADSO-3SD	-24.089	-70.06	4.70E-04	1.00E-04	8.49	22.7	87.6	330.8
ADBA-12SDsm	-23.398	-69.462	5.40E-04	7.00E-05	757.93	26.7	136	634.3

SGC	37.326	-122.387	2.34E-01	2.31E-02	131.56	19.8	98.3	450
PC	37.264	-122.406	2.42E-01	2.28E-02	154.08	19.6	101.5	480.6
WC	37.113	-122.27	2.93E-01	2.68E-02	59.17	24.7	110.9	468.6
SLR	36.972	-122.024	2.11E-01	1.83E-02	303.92	21.9	112.3	524.9
YG07	-30.187	139.428	3.76E-02	4.72E-03	79.09	25.4	119.4	524.2
DCF01	-32.231	137.932	3.13E-02	3.31E-03	38.99	26.9	121.3	517.7
reg-5	49.121	12.121	2.86E-02	4.77E-03	2711.53	9.9	62.1	331.3
reg-7	49.181	12.4	2.76E-02	2.97E-03	2291.15	11.5	69.1	356
reg-11	49.243	12.738	2.31E-02	2.51E-03	385.87	9.5	49.5	231.7
reg-12	49.187	12.736	2.89E-02	3.12E-03	1357.73	15.3	88.3	443.7
reg-12A	49.187	12.736	2.93E-02	3.65E-03	1357.73	15.3	88.3	443.7
reg-12	49.187	12.736	2.93E-02	2.97E-03	1357.73	15.3	88.3	443.7
reg-12D	49.187	12.736	2.82E-02	2.73E-03	1357.73	15.3	88.3	443.7
reg-13	49.171	12.845	3.02E-02	3.11E-03	229.22	21.2	106	479.6
reg-14	49.146	12.838	2.46E-02	2.56E-03	994.38	15.7	89.5	446
reg-18	49.048	13.233	3.24E-02	4.84E-03	160.23	24.3	112.9	484.2
reg-18A	49.048	13.233	3.06E-02	6.71E-03	160.23	24.3	112.9	484.2
reg-18	49.048	13.233	3.15E-02	3.46E-03	160.23	24.3	112.9	484.2
reg-18D	49.048	13.233	3.51E-02	4.35E-03	160.23	24.3	112.9	484.2
reg-19	49.015	13.255	2.75E-02	2.98E-03	108.53	23.8	108.8	462.6
reg-19	49.015	13.255	2.75E-02	3.02E-03	108.53	23.8	108.8	462.6
reg-19	49.015	13.255	2.75E-02	2.94E-03	108.53	23.8	108.8	462.6
reg-20	49.011	13.216	3.25E-02	3.37E-03	294.94	24	113.8	496.9
neck-1	48.179	8.617	5.44E-02	6.28E-03	455.29	7.6	37.9	173.5
neck-2	48.396	8.648	1.02E-01	1.49E-02	789.32	10.5	57.9	284.8
neck-3	48.704	9.419	1.08E-01	1.74E-02	3263.55	11.4	70	368.1
neck-4	48.704	9.419	9.66E-02	1.18E-02	3263.55	11.4	70	368.1
neck-6	49.45	8.936	8.26E-02	6.86E-03	12922.2	8.6	57.2	323
neck-6	49.45	8.936	8.37E-02	9.73E-03	12922.2	8.6	57.2	323
neck-6	49.45	8.936	9.41E-02	6.16E-03	12922.2	8.6	57.2	323
neck-6D	49.45	8.936	7.01E-02	4.70E-03	12922.2	8.6	57.2	323

neck-7	49.31	9.145	1.16E-01	1.20E-02	12399.2	9.7	62.9	348.2
neck-7	49.31	9.145	1.14E-01	1.64E-02	12399.2	9.7	62.9	348.2
neck-7	49.31	9.145	1.18E-01	7.66E-03	12399.2	9.7	62.9	348.2
neck-8	49.004	9.158	1.34E-01	1.65E-02	5600.61	10.5	67.3	367
neck-10	48.854	8.617	5.05E-02	7.43E-03	301.83	19.9	101.7	472.6
meu-1	48.401	5.68	2.61E-02	2.65E-03	886.45	4.7	26.1	129.3
meu-4	49.535	5.1	1.70E-02	2.02E-03	3958.93	4.1	27.9	162.8
meu-7	49.896	4.705	2.08E-02	2.63E-03	9234.75	4	27.8	164.5
meu-9	50.322	4.878	3.54E-02	4.12E-03	12279.7	4.8	34.9	212
meu-10	50.472	5.006	2.70E-02	4.80E-03	14623.8	4.4	31.3	188.5
meu-13	51.033	5.763	2.03E-02	3.03E-03	20726.4	5.4	40.5	249.9
meu-13A	51.033	5.763	2.23E-02	3.90E-03	20726.4	5.4	40.5	249.9
meu-13	51.033	5.763	3.27E-02	4.73E-03	20726.4	5.4	40.5	249.9
meu-13D	51.033	5.763	5.81E-03	4.70E-04	20726.4	5.4	40.5	249.9
meu-14	51.284	6.048	3.79E-02	3.98E-03	24691.9	5.6	41.4	253.7
meu-15C	51.5	6.164	6.07E-02	5.40E-03	24996.3	5.5	41.3	254.8
meu-15C	51.5	6.164	5.67E-02	6.59E-03	24996.3	5.5	41.3	254.8
meu-15C	51.5	6.164	6.47E-02	4.20E-03	24996.3	5.5	41.3	254.8
loi-2	47.419	0.926	4.44E-02	4.84E-03	42144.6	10.3	77.8	468.9
loi-2	47.419	0.926	4.43E-02	6.67E-03	42144.6	10.3	77.8	468.9
loi-2	47.419	0.926	4.45E-02	3.01E-03	42144.6	10.3	77.8	468.9
loi-10	47.001	3.059	3.71E-02	5.29E-03	32697.9	13	87	482.2
loi-11	46.961	3.133	3.06E-02	7.26E-03	18294	11.3	74.8	409.9
loi-12	46.95	3.066	4.53E-02	4.78E-03	14345.9	15.3	102.6	570.6
loi-12	46.95	3.066	4.44E-02	6.38E-03	14345.9	15.3	102.6	570.6
loi-12	46.95	3.066	4.61E-02	3.17E-03	14345.9	15.3	102.6	570.6
loi-14	46.651	3.235	4.68E-02	6.83E-03	13303.8	16.3	106.2	579.2
loi-14A	46.651	3.235	4.97E-02	6.98E-03	13303.8	16.3	106.2	579.2
loi-14	46.651	3.235	4.39E-02	6.67E-03	13303.8	16.3	106.2	579.2
loi-15	46.436	3.328	5.46E-02	7.39E-03	12757.2	17.1	109	586.5
loi-17	46.075	3.455	4.89E-02	4.93E-03	8989.15	18.8	118.4	632.2

loi-18	45.944	3.449	4.49E-02	5.07E-03	1478.59	21.2	120.8	601
loi-19	45.923	3.36	6.90E-02	9.22E-03	6050.14	20.3	128	688.4
loi-21	45.666	3.648	3.63E-02	5.25E-03	759.82	20	108.7	525.3
loi-23	45.462	3.285	5.43E-02	6.03E-03	4117.87	21.9	132	686.6
loi-25	45.117	3.492	5.33E-02	7.02E-03	1805.42	24.4	142.6	731
loi-25A	45.117	3.492	5.12E-02	6.97E-03	1805.42	24.4	142.6	731
loi-25	45.117	3.492	5.54E-02	7.07E-03	1805.42	24.4	142.6	731
loi-33	44.933	3.383	3.95E-02	4.95E-03	10.65	23.6	93.2	353.2
loi-36	44.732	3.862	3.84E-02	5.06E-03	256.08	17.1	85.2	390.8
loi-37	44.867	3.926	8.13E-02	1.19E-02	414.91	21.7	110.8	513.7
loi-40	45.998	4.045	5.55E-02	7.72E-03	6595.51	17.9	113.1	607.2
loi-41	46.487	3.899	3.04E-02	3.76E-03	12703.5	13.6	86.5	461.2
loi-45	47.492	1.285	2.34E-02	2.60E-03	1398.71	1.4	8.6	44.9
loi-48	47.138	3.206	6.42E-03	6.50E-04	200.47	5.2	26	118.6
loi-49	47.036	3.207	1.27E-02	1.25E-03	554.97	5.5	29.4	140.2
loi-50	46.837	3.501	2.11E-02	2.02E-03	1678.95	5.2	29.1	144.2
loi-51	46.771	3.45	1.21E-02	1.30E-03	383.78	2.8	14.5	69
loi-52	46.517	3.683	2.73E-02	2.75E-03	749.27	13	71.1	344.3
loi-55	46.364	3.314	3.49E-02	3.92E-03	2554.83	15.1	90.9	472
loi-56	46.006	3.459	2.17E-02	2.49E-03	135.34	4.6	23.4	109.5
CS-03	36.466	-80.834	1.45E-02	1.15E-03	89.72	19.5	88.6	377.8
CS-03A	36.466	-80.834	1.44E-02	1.15E-03	89.72	19.5	88.6	377.8
CS-03B	36.466	-80.834	1.46E-02	1.17E-03	89.72	19.5	88.6	377.8
CS-03C	36.466	-80.834	1.68E-02	1.32E-03	89.72	19.5	88.6	377.8
CS-03D	36.466	-80.834	1.21E-02	9.60E-04	89.72	19.5	88.6	377.8
CS-16	35.542	-82.381	1.56E-02	1.24E-03	11.06	22.1	93.5	379.6
CS-19	35.636	-82.219	3.30E-02	2.50E-03	6.43	25.5	101.6	392.5
CS-20	35.621	-82.179	2.88E-02	2.28E-03	35.12	24.2	109.2	466.4
CS-21	35.584	-82.164	2.25E-02	1.70E-03	47.39	17.4	75.5	309.1
CS-25	36.717	-80.433	8.46E-03	7.60E-04	5.28	5.7	21.5	79.5
CS-27	36.76	-80.372	9.93E-03	8.50E-04	8.5	7.9	30.2	113

CS-28	36.785	-80.298	1.73E-02	1.38E-03	6.19	26	103	395.9
CS-29	36.725	-80.226	7.20E-03	6.00E-04	18.17	17.4	71.2	280.8
CS-31	36.664	-80.34	3.45E-02	2.64E-03	5.46	24	95.2	366.2
CS-32	36.616	-80.451	2.49E-02	1.92E-03	116.44	22.5	113.4	528.9
ESP-5	6.72	80.78	3.47E-02	3.85E-03	19.05	83.6	353.8	1432.6
BO-R2F	6.757	80.762	1.22E-02	1.26E-03	23.01	79.5	356.3	1525.8
HG(F)-3	6.926	80.817	9.59E-03	7.90E-04	10.66	13.7	55.9	221.4

Table S5: Sensitivity of morphometrics to data resolution

Site	Basin Area (km ²)	Resolution (m)	Channel Steepness						% of Basin in which channel slope > 0.2
			$\theta = 0.4$		$\theta = 0.5$		$\theta = 0.6$		
			ks(m0.8)	R2	ks(m)	R2	ks(m1.2)	R2	
<i>Venezuela</i>									
RNF-117 / RNNR	208.42	90	1.25	0.83	6.23	0.80	29.22	0.69	0
		250	1.45	0.72	7.14	0.75	32.90	0.73	
		500	1.58	0.70	8.17	0.73	40.25	0.73	
RGF-129 / RGB-130	684.89	90	3.07	0.47	17.09	0.43	86.19	0.37	0.104
		250	3.32	0.44	18.28	0.42	90.10	0.37	
		500	3.83	0.46	21.99	0.44	116.23	0.41	
<i>Brazil</i>									
BR-UB-RS1	19.9	90	59.79	0.91	222.78	0.86	817.51	0.80	0.654
		250	50.61	0.91	210.34	0.87	833.39	0.78	
		500	61.60	0.91	275.20	0.92	1,193.28	0.91	
BR-UB-RS4	3.183	90	5.44	0.81	21.81	0.78	86.20	0.73	0
		250	8.51	0.33	33.58	0.41	128.56	0.47	
		500	10.66	0.51	42.23	0.53	165.57	0.55	
BR-UB-RS5	11.129	90	4.68	0.35	19.15	0.35	76.91	0.34	0
		250	8.39	0.37	33.40	0.44	128.92	0.49	
		500	10.15	0.50	41.11	0.51	163.91	0.51	
BR-UB-RS6	0.6	90	16.00	0.89	54.14	0.88	182.27	0.88	0
		250	21.15	-0.04	70.92	0.00	236.22	0.03	
		500	48.10	1.00	173.78	1.00	626.10	1.00	
BR-UB-RS7	35.373	90	53.98	0.80	242.74	0.71	1,040.64	0.57	0.731
		250	59.12	0.74	258.83	0.64	1,072.03	0.46	
		500	68.65	0.76	317.55	0.69	1,417.39	0.59	
BR-UB-RS8	10.959	90	25.86	0.87	108.67	0.83	439.50	0.73	0.191
		250	32.04	0.83	132.46	0.85	526.04	0.83	
		500	38.04	0.80	166.78	0.84	715.62	0.87	
<i>Guatemala</i>									
		90	57.33	0.95	228.18	0.91	885.75	0.84	

GT-62	5.168	250	68.02	0.88	258.47	0.82	956.81	0.73	0.762
		500	82.74	0.79	357.95	0.76	1,522.07	0.71	
Costa Rica									
Rio Cedro	43.829	90	60.87	0.91	275.26	0.83	1,193.69	0.71	0.576
		250	63.70	0.93	280.52	0.85	1,174.78	0.73	
		500	76.29	0.90	351.87	0.84	1,569.52	0.75	
Rio Hamaca	29.176	90	59.90	0.89	266.81	0.78	1,130.78	0.58	0.531
		250	61.88	0.87	267.15	0.75	1,090.02	0.56	
		500	72.25	0.92	331.20	0.87	1,470.32	0.78	
Taiwan									
TW-RS1	1.393	90	59.79	0.91	222.78	0.86	817.51	0.80	1
		250	68.45	0.93	248.58	0.91	886.04	0.87	
		500	83.21	0.91	318.77	0.91	1,211.53	0.91	
TW-RS2	523.074	90	80.81	0.83	414.63	0.67	1,897.95	0.32	0.842
		250	93.23	0.83	474.33	0.74	2,181.07	0.49	
		500	105.72	0.84	570.95	0.81	2,871.98	0.67	
TW-RS3	535.556	90	71.19	0.85	374.94	0.79	1,805.48	0.62	0.813
		250	77.74	0.85	395.98	0.79	1,828.91	0.62	
		500	87.32	0.84	470.67	0.82	2,361.30	0.72	

Table S6: Summary of precipitation records from representative stations for cosmogenic radionuclide study sites

Sample Name	Sample Location		Station identifier	Data Source	Station Location		Mean annual precipitation (mm)	Simple daily intensity index (mm/day)	Daily Precipitation		Average maximum peak-to-mean ratio	Start of record	End of record	Number of days with precipitation	Number of days in record
	Longitude	Latitude			Longitude	Latitude			90th percentile (mm)	99th percentile (mm)					
<i>Venezuela</i>															
RNF-117	-61.116	7.42	VE000080453	GHCN	-61.45	7.30	425.10	9.9	10.9	45.0	8.7	1973	1997	1231	2463
RNNR	-61.142	7.397	VE000080453	GHCN	-61.45	7.30	425.10	9.9	10.9	45.0	8.7	1973	1997	1231	2463
RGF-129	-61.687	8.106	VE000003994	GHCN	-62.38	8.02	981.90	8.7	20.8	52.7	7.3	1950	1996	6991	15236
RGB-130	-61.692	8.11	VE000003994	GHCN	-62.38	8.02	981.90	8.7	20.8	52.7	7.3	1950	1996	6991	15236
<i>Brazil</i>															
BR-UB-RS1	-44.838	-23.339	BR002345067	GHCN	-45.14	-23.33	1878.80	13.8	32.0	95.8	9.1	1936	1995	10543	20167
BR-UB-RS4	-45.097	-23.332	BR002345067	GHCN	-45.14	-23.33	1878.80	13.8	32.0	95.8	9.1	1936	1995	10543	20167
BR-UB-RS5	-45.093	-23.329	BR002345067	GHCN	-45.14	-23.33	1878.80	13.8	32.0	95.8	9.1	1936	1995	10543	20167
BR-UB-RS7	-45.023	-23.389	BR002345067	GHCN	-45.14	-23.33	1878.80	13.8	32.0	95.8	9.1	1936	1995	10543	20167
BR-UB-RS8	-44.965	-23.375	BR002345067	GHCN	-45.14	-23.33	1878.80	13.8	32.0	95.8	9.1	1936	1995	10543	20167
<i>Guatemala</i>															
GT-62	-89.694	15.088	HO000078714	GHCN	-88.86	14.83	1404.60	9.5	22.7	55.8	7.1	1979	1993	2894	5479
<i>Costa Rica</i>															
Rio Cedro	-82.888	8.985	CSM00078762	GHCN	-84.209	9.994	1294.90	14.0	22.9	59.4	7.2	1986	2018	3595	5888
Rio Hamaca	-82.925	8.984	CSM00078762	GHCN	-84.209	9.994	1294.90	14.0	22.9	59.4	7.2	1986	2018	3595	5888
<i>Taiwan</i>															
TW-RS1	121.841	24.497	467060	GSOD (USAF)	121.85	24.60	1750.70	15.0	39.1	133.0	10.7	1982	1998	2331	6140
TW-RS2	121.594	24.174	466990	GSOD (USAF)	121.60	23.98	833.60	12.5	28.9	137.9	12.2	1973	1998	2203	9293
TW-RS3	121.737	24.322	466990	GSOD (USAF)	121.60	23.98	833.60	12.5	28.9	137.9	12.2	1973	1998	2203	9293